Arlin Gruber BSc

Model based approach to detect critical process and material parameters on a pharmaceutical manufacturing process

MASTER'S THESIS

to achieve the university degree of

Master of Science

Master's degree programme: Biomedical Engineering

submitted to

Graz University of Technology

Supervisors

Univ.-Prof. Dipl.-Ing. Dr.techn. Christian Baumgartner,

Assoc.Prof. Dipl.-Ing. Dr.techn. Jörg Schröttner

Institute of Health Care Engineering, TU Graz

Stremayrgasse 16/II, 8010 Graz

Univ.-Prof. Dipl.-Ing. Dr.techn. Johannes Khinast

Institut für Prozess- und Partikeltechnik, TU Graz

Inffeldgasse 13/III, 8010 Graz

Graz, August 2018

Table of Content

Statutory Declaration

EIDESSTATTLICHE ERKLÄRUNG
AFFIDAVIT

Ich erkläre an Eides statt, dass ich die vorliegende Arbeit selbstständig verfasst, andere als die angegebenen Quellen/Hilfsmittel nicht benutzt, und die den benutzten Quellen wörtlich und inhaltlich entnommenen Stellen als solche kenntlich gemacht habe. Das in TUGRAZonline hochgeladene Textdokument ist mit der vorliegenden Masterarbeit/Diplomarbeit/Dissertation identisch.

I declare that I have authored this thesis independently, that I have not used other than the declared sources/resources, and that I have explicitly indicated all material which has been quoted either literally or by content from the sources used. The text document uploaded to TUGRAZonline is identical to the present master‘s thesis/diploma thesis/doctoral dissertation.

Datum/Date	Unterschrift/Signature

Die Technische Universität Graz übernimmt mit der Betreuung und Bewertung einer Masterarbeit keine Haftung für die erarbeiteten Ergebnisse: Eine positive Bewertung und Anerkennung (Approbation) einer Arbeit bescheinigt nicht notwendigerweise die vollständige Richtigkeit der Ergebnisse.

Abstract

Direct compaction represents a major operation within the pharmaceutical industry. In the pharmaceutical industry it is crucial to meet pre-defined product properties. In order to meet the desired product quality, it is essential to know which model inputs and process parameters contribute to critical quality attributes. Sensitivity analysis allows to study how the uncertainty in a model output can be apportioned to different sources of uncertainty in its inputs, by statistically evaluating the results of many simulations. Utilizing variance-based sensitivity analysis has gained popularity in many research fields of engineering. In this work, sensitivity analysis is applied to a direct compaction process, where variance-based sensitivity measures, in particular Sobol's method in combination with Morris method, will quantify these influences. Based on the results, a reduction of model complexity can be achieved by neglecting insignificant model inputs. The work aims at exploiting the possibilities to use the advantages of each method to demonstrate the potential benefits of a combination of both, to detect, quantify and rank influential parameters on a continuous direct compaction process.

Keywords

Model-based approach, process simulation, global sensitivity analysis, Sobol' method, Morris method

Kurzfassung

Direktkompaktierung stellt einen wichtigen Prozessschritt in der pharmazeutischen Industrie dar. Gerade in der pharmazeutischen Industrie ist es von enormer Wichtigkeit, vordefinierte Produkteigenschaften einzuhalten. Um die gewünschte Produktqualität zu gewährleisten, ist es wesentlich zu wissen, welche Modelleingänge und Prozessparameter sich auf kritische Qualitätsattribute auswirken. Sensitivitätsanalyse erlaubt durch statistische Evaluierung von vielen Simulationsläufen, die Varianz einer Modell Ausgangsgröße unterschiedlichen Unsicherheitsquellen im Modell Eingang zuzuordnen. Die Verwendung von Varianzbasierter Sensitivitätsanalyse hat große Verbreitung in vielen Forschungsfeldern des Ingenieurwesens gefunden. In dieser Arbeit wird Sensitivitätsanalyse am Prozess der Direktkompaktierung angewandt, wobei varianzbasierte Sensitivitätsgrößen, im speziellen die Sobol‘ Methode in Kombination mit der Morris Methode, die Quantifizierung von kritischen Einflussgrößen erlaubt. Basierend auf den Ergebnissen kann eine Reduktion der Modelkomplexität erreicht werden, die auf einer Vernachlässigung von Modellgrößen beruht. Diese Arbeit zielt darauf ab, die Möglichkeiten und Vorteile jeder Methode zu demonstrieren und mittels deren Kombination kritische Material- und Prozessgrößen zu erkennen, quantifizieren und entsprechend ihrem Einfluss zu reihen.

Keywords

Model-basierter Ansatz, Prozesssimulation, Globale Sensitivitätsanalyse, Sobol’ Methode, Morris Methode

Acknowledgement

The execution of this master thesis would not be possible without the support of some people; therefore, I want to express my gratitude to all of you.

First, I would like to express my gratitude to RCPE GmbH and Prof. Khinast, for providing me with the opportunity to do my master's thesis in such a stimulating and challenging environment. A big thank you goes to Prof. Baumgartner and Prof. Schröttner for their supervision of my master thesis.

A special thanks goes to Jakob Rehrl and Michael Martinetz, to whom I am grateful for their scientific advice. I appreciate your support, your honest feedback and the numerous discussions we had.

I also want to say thank you to my friends, who always distracted and supported me at the same time, for my university work and made my life much easier.

Last but not least, I am grateful for having such a wonderful family who offered me the possibility of studying in Graz. Without your trust and support it would not have been possible to accomplish my studies.

1. Introduction

1.1. Pharmaceutical solid dosage processes

Continuous manufacturing (CM) gets increased attention within the pharmaceutical industry since it offers several advantages compared to batch-wise manufacturing. The manufacturing of pharmaceutical dosage forms is traditionally a batch-wise process. Scale-up of the batch size processes could lead to problems, since the involved equipment does not facilitate to the scale-up process. As an alternative continuous or semi-continuous processes have been introduced to enhance process stability within closed and compact units, with a high degree of automation. Therefore, the sequential batch processes are integrated into a continuous process which could run 24/7 with fewer manual interventions. In CM materials are non-stop and uninterrupted processed through a plant until a final product is completed. Within the plant all unit operations are subsequently connected allowing real-time monitoring of process parameters and intermediate quality attributes. It enables a shortened time-to-market of the pharmaceutical product and an increased production volume without the current problems related to scale-up. CM allows to develop wide ranges of novel solid dosage forms where raw materials are seamlessly converted to a final product. The risk of human errors can be reduced with basically no need for equipment shut-down and extensive alterations of the process.

1.1.1. Direct compaction

Pharmaceutical manufacturing comprises often many unit operations, such as feeding, granulation, drying, blending and tableting which are aimed to increase processability of the ingredients [1,2]. Direct compaction (DC) is the preferred choice for tablet manufacturing since it is the simplest form of oral dosage production as it contains the fewest process stages. The production of tablets by direct compaction requires just three process stages. Figure 1 depicts the process steps, where the ingredients are fed, blended and then directly compacted. Such a system has as much feeders as the number of processed components of the pharmaceutical blend. The materials are fed into a blender, from where the homogeneous mixture is transferred into a hopper unit. Through a feed frame the material is entering the subsequent tablet press, where it is compacted into tablets of certain characteristics. In some cases, an additional coating can be applied to the finished tablets.

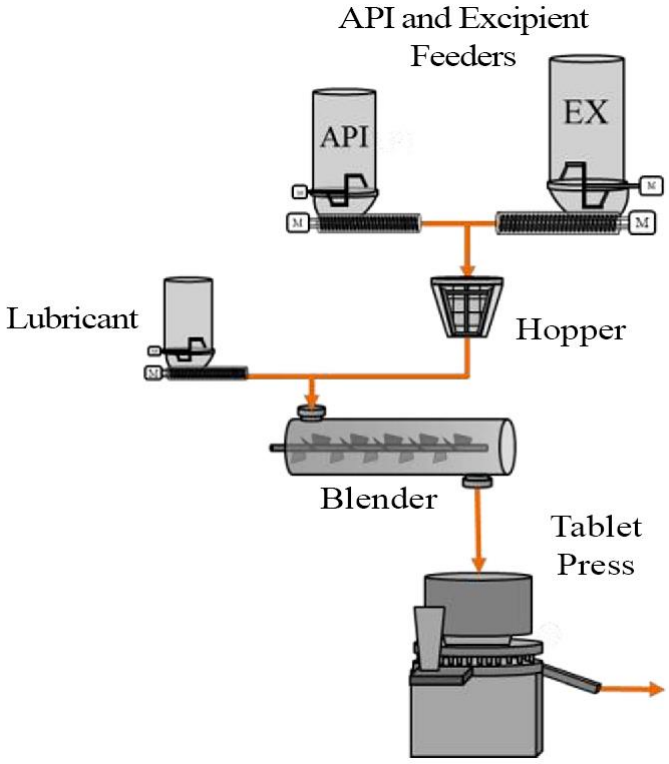

Figure 1: Pharmaceutical direct compaction line in its simplest form (edited from [3]).

1.2. Process simulation

The ICH Q8 guidance for pharmaceutical development describes process modelling and simulation during the process development as an important component of the quality by design (QbD) approach [4]. Computer aided simulation tools, like the process simulation environment gProms, allow to perform analysis on process impact on the end-product. Such analysis methods include global sensitivity analysis and the tracking of material properties along the process. In the gProms landscape, modeling and simulation of solid based processes is possible. The gProms environment allows simulation of process/flowsheet models which can be used to reduce experimental effort during establishing of new processes, enhance scientific understanding and develop control strategies to predict the behavior of a system under a set of conditions.

Process models can be used in order to confirm that the process can reliably deliver products of a determined standard. These standards can be assured by keeping track of critical quality attributes (CQA) throughout the process. CQAs are chemical, physical, biological and microbiological attributes that can be defined, measured, and continually monitored to ensure final product outputs remain within acceptable quality limits [4]. CQA are an essential aspect of a manufacturing control strategy and should be identified early on. Critical process parameters (CPP) on the other hand are operating parameters of the plant that are considered essential for maintaining a product output within specified quality target guidelines. Process simulation is a tool that can provide a link between material attributes and process parameters to a drugs quality profile.

As an example, Boukouvala et al. used integrated process simulation with gProms and applied global sensitivity analysis (GSA) to two tablet manufacturing case studies, to identify challenges in process development via simulation [5]. They were using GSA as part of a holistic approach, integrating the results from sensitivity analysis to establish a control strategy of the process. The GSA results lead to important conclusions about the quantification of uncertainty of specific outputs and how they can be apportioned to different sources of uncertainty of its inputs. The GSA concluded, that input fluctuations were considered potentially critical, since they can lead the process to operate outside the defined design space, where the end-product is no longer meeting defined quality criteria. Knowing the relationship between material and process parameters and the effect of uncertainty regarding critical quality attributes, allows to establish a design space describing ranges of material attributes and process parameters, or more complex mathematical relationships [4] [5].

In another example, sensitivity analysis with two different approaches was introduced to a pharmaceutical direct compaction manufacturing process [6]. The used approaches included the implementation of sensitivity analysis based on Sobol indices with a framework including gProms, MATLAB and the free licensed GSA software SimLab. For comparison a second method based on the steady-state gains and the frequency response of the plant model was yielding similar results. The results provided by both methods made it possible to gain insight how the output can be apportioned to different sources of uncertainty in its inputs and accordingly assign actuating signals to controlled variables.

Process simulation in the field of process development and optimization of control approaches has be widely discussed in literature. As an example: Cotabarren et al., used flowsheet modelling and process simulation to implement a feedback control strategy for a continuous industrial fluidized-bed granulation process, using the gProms development environment [7]. In a previously performed sensitivity analysis they demonstrated that it was possible to determine influential process parameters for their control design. Further promising applications on complex pharmaceutical processes, regarding more advanced control approaches such as MPC, where mathematical models are used for predicting the effects of disturbances and changes of CPPs on CQAs are described in [8, 9]. With these process models describing the real plant behavior it is therefore possible to calculate and predict intermediate quality attributes without actual measuring.

1.2.1. Material tracking

For batch-wise processes where a specific quantity or other material is intended to have uniform character, it is relatively easy to track material properties along all manufacturing units. With CM it has to be assured, that a specific identifiable amount of product in a unit of time, stays within its specified limits. This is no longer trivial, since material is simultaneously charged and discharged from the process and no regulatory guidance regarding CM is established, yet. The FDA only references to the definition of "lot's" regarding batch-wise and continuous processes [10,11]. Material tracking is especially crucial regarding the regulatory approval of continuous manufactured pharmaceutical products [12]. Tracking of material properties along the process allows knowing the physical location of a particular good. To ensure that the end-product is within its quality target product profile QTPP it is necessary to know, whether an intermediate CQA is within its specified limits to take counter measures. In case a known quantity is out-of-specification it can be ejected from the process.

To establish robust manufacturing processes in compliance within the regulatory framework it is necessary to track material characteristics along the process. It is foreseeable, that a combination of both process models and PAT, as well as the implementation of control strategies will lead the way to establish such goals. Nevertheless, the implementation of models capable for material tracking is still in an early phase and will progress further. The implementation of the hopper model described in 2.2. is a step towards this direction.

1.2.2. Aim of the thesis

The aim of the thesis is to showcase how sensitivity analysis can be applied to a direct compaction process. Variance-based sensitivity measures, in particular Sobol's method in combination with Morris method, will quantify uncertainty in the process and material parameters. The work aims at exploiting the possibilities to use the advantages of each method to demonstrate the potential benefits of a combination of both. With both set-ups in place it will be possible to detect, quantify and rank influential parameters on a continuous direct compaction process.

The thesis objectives include:

- Development and modelling of a hopper model as part of the direct compaction process flowsheet.

- Use of global sensitivity analysis (Sobol' and Morris method) for the identification of important properties of the model response that are associated with process understanding.
- Comparison of both methods and investigation of the convergence for the Sobol' method.

1.3. Global sensitivity analysis

Global system analysis is an approach for determining the impact of input uncertainties onto uncertainty of an output quantity of interest in a certain physical or mathematical model. Global sensitivity analysis forward referred as GSA is a method which permits the investigation of the global behavior of a system. In contrast to a single simulation, in which a system equation is solved, in GSA it is possible to specify ranges of the inputs and therefore obtain output distributions over a whole set of multiple simulations. Compared to the execution of a single simulation where a simulation run is based on one input data set, GSA is permitting the investigation of the global behavior of a system based on statistics. In GSA usually all of the parameters are varied simultaneously over their entire parameter range. This allows to evaluate the relative contribution of each individual parameter as well as the interaction among the parameter set to the variance of the model output [13]. This is done with variance analysis, where an observed variance (deviation of a variable from its mean) in a particular variable is partitioned into components attributable to different sources of variation in the inputs.

Global sensitivity analysis is superior to other SA methods, which might be based on correlation or regression coefficients, because of its model independence. GSA works for non-linear and non-additive models, unlike linear regression. To date, several types of global sensitivity analysis such as, Fourier amplitude (FAST), Morris and Sobol's method are applicable for linear or non-linear models [13]. This section introduces the Morris and the Sobol method, since these types of analysis are two of the most commonly used methods for sensitivity analysis.
Global sensitivity analysis has become important to investigate the relations between inputs and outputs of a model simulation. This approach is used among different models and is widely used in different fields of research, where a large amount of variability in critical parameters would not be tolerated. The application of GSA can be found wherever models are used to simulate natural or artificial systems, such as chemical, biological, mechanical or more abstract processes in economics [14],[5]. Despite the increasing interest there have been very few publications regarding pharmaceutical process models. For model-based applications, GSA could become part of a holistic approach to establish functional process control. This study offers two different approaches to get further process insight to pave the way for advanced process control.

1.3.1. Sobol's sensitivity indices

The rapid development of computational capacity and speed of computers has led to an increase of computer aided design of real systems. Although Sobol's method requires high computational costs, it is more effective in capturing interactions between large numbers of variables in highly non-linear models compared to other approaches [15,16].The general workflow for Sobol's sensitivity analysis is shown in Figure 2. Sobol's method is a model independent global sensitivity analysis approach which is based on the decomposition of variance. It is possible to handle non-linear and non-monotonic functions and models [17].

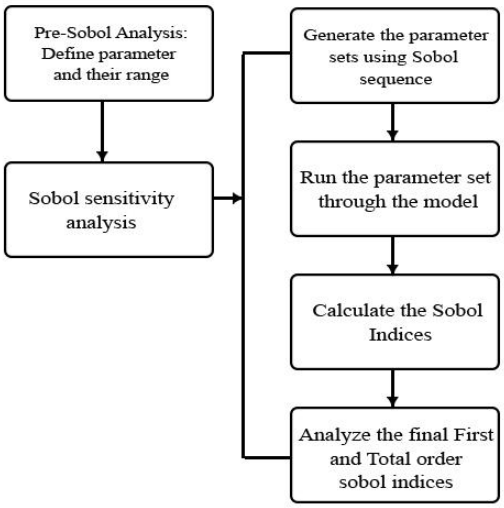

Figure 2: Flow chart of a Sobol sensitivity analysis showing the involved steps (edited from [4]).

A model could be represented by the function:

$$Y = f(X) = f(X_1, \dots, X_k) \quad \text{(Eq. 1)}$$

Where Y is a model output which is dependent on the input vector $X = (X_1, \dots, X_k)$, with k being the total number of independent factors. Sobol's method is based on the decomposition of the variance into summands of different dimensions. The dimensions are the contributions from effects of single parameters (first effect) and combined effects of pairs of parameters (higher-order effects). Based on the assumption that the inputs are uniformly and independently distributed within a unit hypercube, it may be decomposed in the following way:

$$Y = f(X_1, \dots, X_k) = f_0 + \sum_{i=1}^{k} f_i(X_i) + \sum_{i=1}^{k} \sum_{j=i+1}^{k} f_{i,j}(X_i, X_j) + f_{1,\dots,k}(X_1, \dots, X_k) \quad \text{(Eq. 2)}$$

Equation 2 is called analysis of variance (ANOVA) representation of $f(x)$ with equation 3 describing the condition for the described decomposition.

$$\int_0^1 f_{i_1,..,i_s}(X_{i_1},\dots,X_{i_s})\ dX_k = 0 \quad for\ k = i_1,\dots,i_s \tag{Eq. 3}$$

It follows from (3) that the members in (2) are orthogonal and can be expressed as integrals of $f(x)$ [18].

The variance decomposition $V(Y)$ in equation 4, shows how the variance of the model output can be decomposed into terms which are attributable to each input, as well as to interactions among them. For the subsequent equations the average is related to expectation value $E(\cdot)$. Terms of higher-order interaction indices can be calculated by dividing the variance decomposition by V(Y).

$$V(Y) = \sum_{i=1}^{k} V_i + \sum_{i=1}^{k}\sum_{j=i+1}^{k} V_{i,j} + \cdots + V_{1,\dots,k} \tag{Eq. 4}$$

$$V_i = V_{X_i}(E_{X_{\sim i}}(Y|X_i)) \tag{Eq. 5}$$

In equation 6, $\mathrm{V}_{\mathrm{X_{i,j}}}\left(E_{X_{\sim i,j}}(Y|X_i,X_j)\right)$ measures the joint effect of the pair (X_i,X_j) on Y. The $X_{\sim i}$ notation indicates a set of all variables except X_i. In the term of $V_{X_{i,j}}\left(E_{X_{\sim i,j}}(Y|X_i,X_j)\right)$, the inner average $E_{X_{\sim i,j}}(Y|X_i,X_j)$ is evaluated over the space of all factors but X_i, X_j. and the outer variance over all possible values of X_i, X_j. The term $V_{i,j}$ is the joint variance of X_i and X_j. minus the first-order effects for the same factors.

$V_{i,j}$ is used to compute the second-order contribution from interaction between the i_{th} and j_{th} parameters. Together, all terms of the first and higher order variances, sum up to the total variance of the model output [19].

$$V_{i,j} = V_{X_{i,j}}\left(E_{X_{\sim i,j}}(Y|X_i,X_j)\right) - V_i - V_j \tag{Eq. 6}$$

$$V_{i,j,k} = V\left(E(Y|X_i,X_j,X_k)\right) - V_i - V_j - V_k - V_{ij} - V_{jk} - V_{ik} \tag{Eq. 7}$$

The first-order sensitivity index S_i, represents the fractional contribution of a given factor X_i to the variance of a output variable Y [20]. The ratios defined by equation 8, are called global sensitivity indices and are all non-negative values [18].

$$S_{i,\dots,k} = \frac{V_{i,\dots,k}}{V(Y)} \tag{Eq. 8}$$

The first-order indices, sometimes also referred as main effect of X_i , are normalized by the total variance to provide a fractional contribution. As an example, $S_i = \frac{V_i}{V(Y)}$ provides the first-order

contribution from the i_{th} input parameter to the output variance $V(Y)$. $S_{i,j} = \frac{V_{i,j}}{V(Y)}$ is used to compute the second-order contribution from an interaction between the i_{th} and j_{th} parameter. Finally, by dividing both sides of equation 4 with $V(Y)$, equation 9 can be obtained.

$$\sum_{i=1}^{k} S_i + \sum_{i=1}^{k} S_{i,j} + \cdots + S_{1,\ldots,k} = 1 \quad \text{(Eq. 9)}$$

A model without interactions is said to be additive in its factors. For a purely additive model and orthogonal inputs, the first order indices would be:

$$\sum_{i=1}^{k} S_i = 1 \quad \text{(Eq. 10)}$$

Using the first-order indices S_i and higher-order indices $S_{i,j}$ and $S_{1\ldots k}$ given above, it is possible to build a picture of the importance of each variable contributing to the output variance. In case the number of variables is large, calculating the higher-order indices can be very computationally demanding and is prohibitive for complex model simulations. Calculating the higher-order indices by a "brute force" approach requires solving of multidimensional integrals in the space of the input factors [19].

Therefore, a measure known as the total-order index S_{Ti}, is used. The calculation of S_{Ti}, can be based on the variance $V_{\sim i}$ that results from the variation of all parameters, except X_i [21]. This measures the contribution to the output variance of X_i and includes all variances caused by its interactions with any other input variables and of any order.

$$S_{T_i} = 1 - \frac{V_{\sim i}}{V(Y)} \quad \text{(Eq. 11)}$$

The total sensitivity index S_{T_i}, which is related to the input factor of interest, is defined as the sum of all effects (including first-order and higher-order effects) [22]. S_{T_i} is a measure of the contribution to the output variance of X_i, which is including all variance caused by its interactions (of any order) with any other input variables.

$$S_{T_i} = \frac{V(Y) - V_{X_{\sim i}}(E_{X_i}(Y|X_{\sim i})}{V(Y)} = 1 - \frac{V_{X_{\sim i}}(E_{X_i}(Y|X_{\sim i})}{V(Y)} \quad \text{(Eq. 12)}$$

Unlike the first-order indices, the sum of S_{T_i} is allowed to exceed one due to the fact that encountered interaction of higher-order indices are additionally taken into account.

$$\sum_{i=1}^{k} S_{T_i} \geq 1 \qquad \text{(Eq. 13)}$$

For a purely additive model $S_i = S_{T_i}$ and the sum of the S_{T_i} will only be equal to 1, while for a given factor X_i an important role of interaction is flagged by a difference between S_i and S_{T_i} [22] [23].

It is possible to calculate the indices above analytically by evaluating the integrals in the decomposition. From a mathematical point of view, the calculation of the indices is presented by a set of multidimensional integrals. However, in the vast majority of cases they are estimated by a Monte Carlo (MC) approach. Finding an analytical solution is often too complex, leading to efficient approaches by evaluating numerically with MC. The Monte Carlo approach requires the generation of a sequence of randomly distributed points inside a unit hypercube. In practice usually random sequences are substitute with low-discrepancy sequences to improve the efficiency of the estimators, known as quasi-Monte Carlo method [13,24].
In order to calculate both indices, there are a number of possible Monte Carlo estimators available. For an in depth analysis of the most commonly used estimators, it is advisable to read [25], [26]. The Monte Carlo estimate of the partial output variance is:

$$\hat{V}(Y) = \frac{1}{N} \sum_{m=1}^{N} f^2\left(x^{(m)}\right) - \hat{f_0}^2 \qquad \text{(Eq. 14)}$$

where $\hat{V}$ stands for the estimate, f is the function representing the model (or objective function), $x^{(m)}$ is a sampled set of the k parameters X_i, N is the number of samples and ${f_0}^2$ is the square of the expectation value of f.
To compute the Monte Carlo integrals, Saltelli et al. [25] suggest to use two independent matrices (a 'sample' matrix M_1 and a 'resample' matrix M_2 as shown in Figure 3) with a size of $N \cdot k$. With N corresponding to the number of evaluation runs and k to the number of input parameters. Every row in the matrices represents a possible parameter combination for the model, symbolized as respectively $x^{(1)(m)}$ and $x^{(2)(m)}$.

$$\text{Sobol}(4,3) = \left[\begin{array}{ccc|ccc} 0.5 & 0.500 & 0.500 & 0.500 & 0.375 & 0.750 \\ 0.25 & 0.750 & 0.250 & 0.350 & 0.125 & 0.500 \\ 0.75 & 0.250 & 0.750 & 0.150 & 0.625 & 0.250 \\ 0.125 & 0.625 & 0.875 & 0.475 & 0.125 & 0.375 \end{array}\right]$$

M_1 M_2

For $i = 1$:

$$x_{\sim i}^{(1)(m)} = \begin{matrix} 0.500 & 0.500 \\ 0.750 & 0.250 \\ 0.250 & 0.750 \\ 0.625 & 0.875 \end{matrix} \quad x_i^{(1)(m)} = \begin{matrix} 0.500 \\ 0.250 \\ 0.750 \\ 0.125 \end{matrix} \quad x_{\sim i}^{(2)(m)} = \begin{matrix} 0.375 & 0.750 \\ 0.125 & 0.500 \\ 0.625 & 0.250 \\ 0.125 & 0.375 \end{matrix} \quad x_i^{(2)(m)} = \begin{matrix} 0.500 \\ 0.350 \\ 0.150 \\ 0.475 \end{matrix}$$

Figure 3: Example construction of matrix $\boldsymbol{M_1}$ and $\boldsymbol{M_2}$ ($\boldsymbol{k = 3}$, $\boldsymbol{N = 4}$).

Based on M_1 and M_2 different possibilities exist to estimate the square of the expectation value $\hat{f_0}^2$ and the total variance $\hat{V}$. Saltelli et al. [21] suggested to use equation 15 as an estimate for the square of the expectation value for the computation of the first-order index. $x^{(1)(m)}$ is a set of parameters taken from the matrix M_1, $x^{(2)(m)}$ taken from M_2.

$$\hat{f_0}^2 = \frac{1}{N}\sum_{m=1}^{N} f(x^{(1)(m)}) f(x^{(2)(m)}) \qquad \text{(Eq. 15)}$$

The Monte Carlo estimate for the main effect of input parameter X_i is estimated as:

$$\hat{V}_i = \frac{1}{N}\sum_{m=1}^{N} f\left(x_{\sim i}^{(1)(m)}, x_1^{(1)(m)}\right) f\left(x_{\sim i}^{(2)(m)}, x_i^{(1)(m)}\right) - \hat{f_0}^2 \qquad \text{(Eq. 16)}$$

To obtain the Monte Carlo estimate for the total sensitivity index for variable X_i it is needed to obtain its complementary index:

$$\hat{V}_{\sim i} = \frac{1}{N}\sum_{m=1}^{N} f\left(x_{\sim i}^{(2)(m)}, x_i^{(2)(m)}\right) f\left(x_{\sim i}^{(2)(m)}, x_i^{(1)(m)}\right) - \hat{f_0}^2 \qquad \text{(Eq. 17)}$$

The Sobol sensitivity analysis algorithm requires calculating a single value, which requires the use of an objective function. In order to estimate the first order Sobol' indices S_i and total-order Sobol' indices S_{Ti}, for all the parameters a total of $N(k+1)$ model evaluations is required [21,26,27]. In order to sample the matrices, the quasi-random Sobol' sequence was used for a more evenly coverage of the input variable space [25].

For selecting the proper number of evaluations Sarrazin et al. suggest distinguishing three different types of convergence (Figure 4) [28]. Convergence describes the fact that GSA results do not change (or change to a limited degree) when using a different sample of model evaluations (of equal or larger size). Indices below a certain screening threshold, which is arbitrary set to 0.05 are considered negligible [13].

1) Convergence of the sensitivity indices, which is reached if the values of the indices remain stable.
2) Convergence of ranking, which is achieved if the ordering between the parameters remains stable.
3) Convergence of screening, which is reached if the partitioning between sensitive and insensitive parameters remains stable.

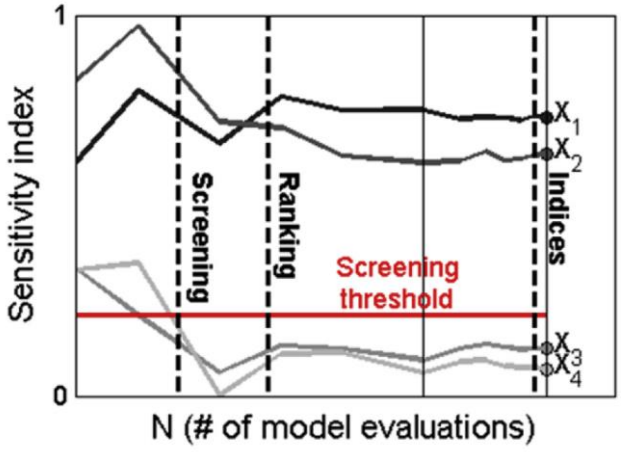

Figure 4: Representation of the three global sensitivity objectives. Figure reports a hypothetical example of four parameters depicting the value of the sensitivity indices against the number of model evaluations [10].

One reason why total Sobol' indices are interesting is interaction among the model parameters [29]. The inputs are interacting when their joint effect on the output is different from the sum of their individual effects. Another advantage of using Sobol indices, is the possibility of applying them to linear and non-linear models, where independent variables could affect the system towards complex and synergetic nonlinear effects. They deliver the impact of variables independent of the assumption of a linear relationship. Sobol' indices also make it possible to compare the variables direct among themselves. However, they provide no information to tendency and the absolute value of the correlation [19].

Another interesting application for GSA is to detect at which point in time a process enters steady-state. By analyzing the dynamic sensitivity profiles it could be observed when the first- or total-order indices remain constant throughout the process. For instance, fluctuations in the sensitivity indices that are evident in the initial stages are resulting from a transition time needed until the system reaches steady-state conditions.

gFormulatedProducts (gFP) provides a development framework for global sensitivity analysis and uncertainty analysis. gFP is built from separate modules which allow the user to select between various methods of sample generation to perform uncertainty and sensitivity analysis executing flowsheet models expressed as mathematical formulas. With a given input data and the calculated results from model evaluation, gFP is capable of computing Sobol's first and total-order indices.

1.3.2. Morris method

The Morris method is commonly used and belongs to the category of screening methods which complements the quantitative methods where the required number of model evaluations is low compared to other GSA techniques [30][26]. The Morris Method is a one-factor-at-a-time (OFAT) method and can be considered as an extension to the local sensitivity analysis. An OFAT method is based on the variation of only one factor while all other factors are kept fixed. Morris method is very efficient in dealing with a large number of model input parameters. The Morris method is an effective way to screen for a subset of relevant parameters among a large number of model parameters. Otherwise these simulations would be high in computational cost and very time consuming. The proposed method is widely used in models of large dimensionality containing hundreds of input factors without relying on strict assumptions to screen factors.

The Morris method is capable of detecting a broad range of effects among model parameters such as negligible parameters, linear, additive or non-linear model behavior. Calculating the statistics of the elementary effects of each input parameter the Morris method allows to detect interactions among parameters [31]. The Morris method is relatively simple to implement and understand with easily interpretable results. It is considered economic in the sense that the required number of model simulations is linear to the number of model factors [32].

To exemplify the Morris method, let us consider a mathematical model with input factors and the output of interest:

$$Y = f(X_1, X_2, \dots X_k) \qquad \text{(Eq. 18)}$$

These two measures are obtained by the construction of a series of trajectories in the input space, where inputs are randomly moved one-at-a-time. Each model input is assumed to vary across in the space of the input factors. The parameter axes are shown in Figure 5 for three input parameters () making up the region of experimentation

The region of experimentation is discretized in a -dimensional -level grid. Each trajectory is composed of points and is designed to build a sample of inputs. The input factors move one by one with a step in while all the others remain fixed. Along each trajectory so-called elementary effects (EE), associated with the i_{th}-input factor are defined as:

$$EE_i(X) = \frac{Y(X_1, \dots, X_{i-1}, X_i + \Delta, X_{i+1}, \dots, X_k) - Y(X)}{\Delta} \quad \text{(Eq. 19)}$$

A trajectory is composed of a successive offset with one input parameter varied at the time. At each step, the offset shifts the input in one dimension only (as depicted in Figure 5). Figure 5 is an example of a three-dimensional input space. The Morris method starts sampling a set of random start values within their defined ranges of possible values for all input variables and performs the model simulation. The second step includes changing the values for one variable, where all of the other inputs remain at their initial values. It then calculates the resulting change in model outcome and compares it to the results of the first run. The same procedure is applied to all other variables and continues until all input variables have been changed. The described procedure is repeated r times, each time with a different set of start values. This leads to $r(k + 1)$ evaluation runs which is more efficient, compared to other more demanding sensitivity analysis methods.

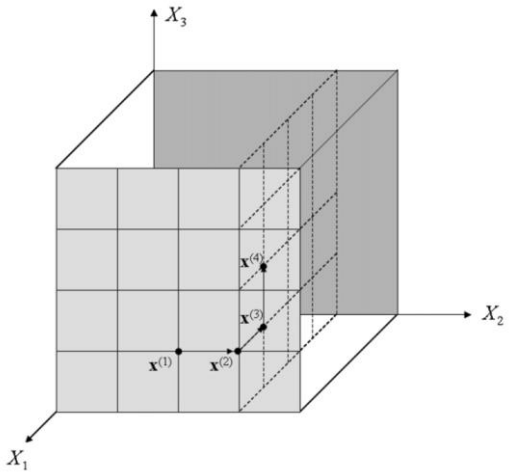

Figure 5: Morris OAT example of a trajectory in a three-dimensional process ($\boldsymbol{k = 3}$, $\boldsymbol{p = 4}$) [33].

The original EE method of Morris [34] provides two sensitivity measures for each input factor:

- assesses the overall influence/importance of an input factor on the model output.
- estimates the ensemble of the factor's higher order effects, describing non-linear effects and interactions.

and are two measures which define for each input the mean and the standard deviation of the distribution of the elementary effects:

$$\mu_i = \frac{1}{k}\sum_{j=1}^{r} EE_i\,(X^{(j)}) \qquad \text{(Eq. 20)}$$

$$\sigma_i = \sqrt{\frac{1}{k-1}\sum_{j=1}^{r}(EE_i(X^{(j)}) - \mu_i)} \qquad \text{(Eq. 21)}$$

The measures described above need to be always considered together to rank input factors in order of importance and for identifying inputs which don't influence the variability of the output. A non-influent input is described by low values of both and Campolongo et al. [35] proposed an improvement of this method by introducing measure which is the mean of the absolute values from the distribution of the elementary effects of the input factors.

$$\mu_i{}^* = \frac{1}{k}\sum_{j=1}^{r}\left|EE_i(X^{(j)})\right| \qquad \text{(Eq. 22)}$$

Using μ^* solves the problem of effects caused by opposite signs which could occur when the model is non-monotonic. A disadvantage of this measure is the loss of information on the sign of the effect. With simultaneous calculation of both measures this information can be recovered at no extra computational cost [35].

Morris et al. [34] proposed a graphical representation in the μ-σ plane to interpret the results, taking the two sensitivity measures into account simultaneously. The standard deviation σ gives information about possible effects between input parameters, with four cases depending on the values of $\mu^*$and σ (Figure 6). A low value for σ and a high value for μ^* implies that the input parameters have a high linear effect on the model output. A low value for μ^* and a high value for σ indicates that the input parameters have a high non-linear effect on the model. With high values for both μ^* and σ, the input parameters show high non-linear effects on the model or strong interactions among them. The considered cases define influential input parameters for the model, which have to be treated with priority [36]. On the other hand, low values for μ^* and σ relate to low effects of the input parameters on the model output.

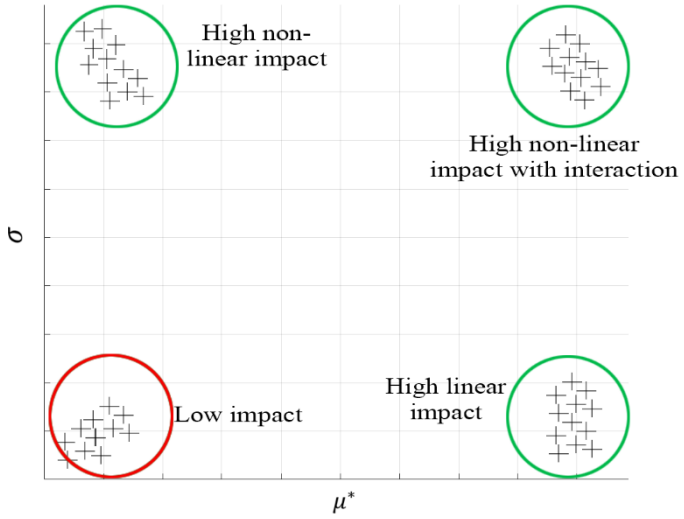

Figure 6: Impact of input parameters according to $\boldsymbol{\mu}^*$ and $\boldsymbol{\sigma}$ (extracted and edited from Loubière et al. [36]).

1.3.3. gFormulatedProducts

For this work, gProms/gFormulatedProducts (Process Systems Enterprise Ltd., United Kingdom) is used as a platform in order to implement the hopper model and to establish the flowsheet of the direct compaction process to simulate both GSA approaches described in 1.3. 1. and 1.3.2.

gProms is widely used throughout the chemicals, energy, petrochemical, power, food and pharmaceutical sectors. It is a multi-purpose tool, using an equation oriented and declarative approach and is mainly used to build and validate process models, comprising steady-state and dynamic simulations among several other functions. The software is suited for large scale non-linear differential algebraic modelling where models can be built by mathematical expressions relating to various physical and chemical variables, without specifying the order in which these equations need to be solved.

For this work, the DC plant model was implemented in a flowsheet type structure, with the models easily accessible for users unfamiliar with advanced mathematical models. The gProms software environment provides pre-developed models via a standard library. It also offers the possibility to create custom libraries of models. gProms offers a good usability with "drag and drop" capability to construct flowsheets.

2. Modelling and simulation

2.1. Flowsheet simulation of the manufacturing process

The direct compaction flowsheet model was developed and implemented according to the experimental set-up of direct compaction line described in [1] and [37]. It consists of three feeders, a blender, a hopper, a tablet press and a subsequent in-vitro dissolution model. In the process development of a new product, an aim is to produce tablets with a fixed dissolution profile and tablet hardness properties as specified in the tablets quality target product profile. The tablet properties are affected by the material properties and changing manufacturing conditions, while processing the powder blend into the final tablet. As described in the previous chapter, understanding the impact of the starting material properties and manufacturing conditions is of high relevance for product development.

The DC line is presented by the process model in Figure 7 which is a model-based representation of the experimental set-up performed by Lakio et. al [37]. The flowsheet is showing all the models which are necessary for the simulation of the real plant. The model parameters are set according to their specification with a tablet target weight of 150mg, compacted in a tablet press at a turret speed of *48* rpm using 7 mm concave punches [37]. Global material attributes such as molecular mass, heat transfer coefficients and settings for the PSD were pre-defined in the global specifications.

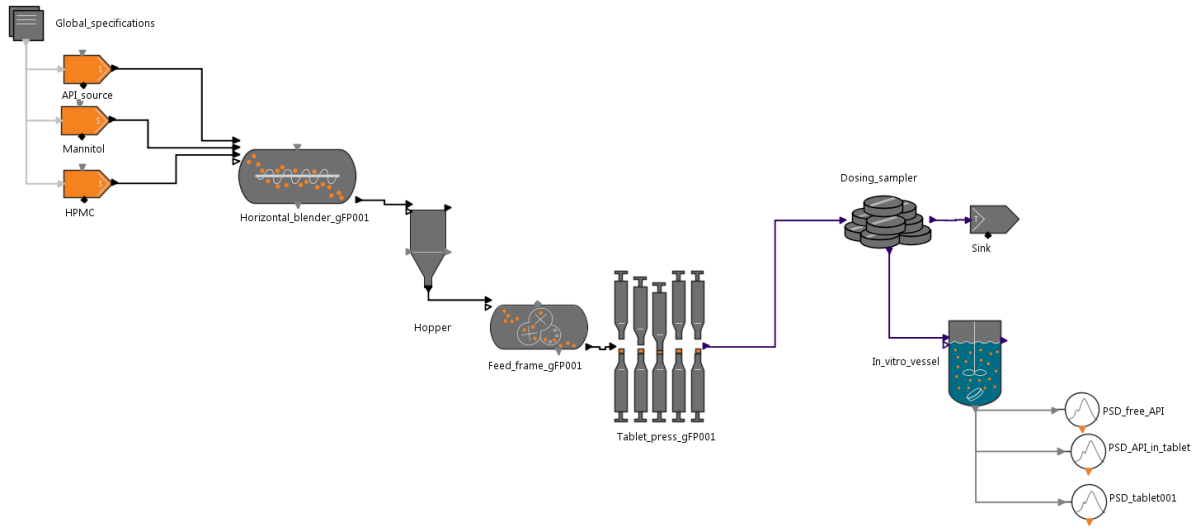

Figure 7: gFormulatedProducts flowsheet of the direct compaction process.

2.1.1. Model inputs and input distributions

The dynamic behavior as well as steady-state performance of the process model depends highly on the assumed ranges of the input parameters. The distribution of the input parameters dictates which values of the input are used for the analysis. In order to apply sensitivity analysis to the simulation model, a first step involves the assignment of probability density functions (e.g. uniform, normal, lognormal, etc.) to the input parameters of the flowsheet model [5]. The model input parameters were selected regarding to Lakio et. al, where their ability to affect quality attributes such as particle size distribution, dissolution profile and the tablet tensile strength was discussed. These simulation inputs include material, process as well as model parameters which are typically underlying a certain uncertainty (Table 1). Generally, most of the process parameters and material attributes could influence quality attributes to some extent, but not all of these process parameters can be monitored and controlled. The ranges of uncertain input parameters were challenged by the design of formulation, including variable powder characteristics and the composition of low and high amounts of API mass fractions. To enhance compaction and powder flow, additionally a relatively low amount of the extended release former (32wt% of HPMC) was used to maximize the amount of filler (Mannitol). With low amounts of matrix former, there is a risk that the formulation might show poor release robustness. This particular conditions, are even more challenging using matrix formers with larger particle sizes, which are more suitable for DC processes leading to the investigation of PSD_{HPMC}.

Without prior knowledge of the parameters distribution, a uniform distribution with lower and upper values is assigned to the model inputs [5], [38]. The ranges of the probability density functions are selected according to the available knowledge provided in [37]. Due to the unknown PDF of the input parameters, this study uses uniform distributions for all of the input parameters. Nevertheless, the PSD is log-normal distributed since not the distribution itself, but rather the location of the mean value is uniformly distributed. Since the powder characteristic affects a lot of critical quality attributes of the end-product, a lot of effort is put in understanding the effects of material properties used for manufacturing of solid dosage forms [1], [39]. For this work, the particle sizes (μ_{API}, μ_{HPMC}) of two solid phases are considered subjects to uncertainty regarding the material parameters. The upper and lower boundaries are picked according to their nominal values with a ±20% tolerance.

Table 1: Input parameters for the compaction process flowsheet

Parameter	Description	Unit	Lower	Upper	Distribution
Material parameters					
μ_{API}	PSD of API, location parameter	µm	30	80	Uniform
μ_{HPMC}	PSD of HPMC, location parameter	µm	70	120	Uniform
Process parameters					
F_{comp}	Compaction force of the tablet press	kN	6	8	Uniform
$\omega_{blender}$	Rotation rate of the blender	rpm	300	1200	Uniform
$\dot{m}_{API}$	Mass flow rate API	kg/h	0.07	0.77	Uniform
$\dot{m}_{Mannitol}$	Mass flow rate Mannitol	kg/h	1.54	2.24	Uniform

Usually the range of input values has more influence on the output than the shape of the distribution itself [40]. Other studies seemed to confirm this statement [41,42]. By using a uniform distribution, the unimportant parameters still show some influence regardless of their distribution. In case the distribution can't be determined, a uniform distribution can be used to ensure an even coverage of the factors space. For an even more accurate sensitivity analysis, the parameter distributions can be estimated from experimental data, which is not always easy to obtain [38,43].

Table 2 depicts the CQAs which should be influenced by a variation among the distributions in the model inputs. These quality attributes are critical to the solid-dosage end-product and have to stay within a narrow fluctuation margin. The CQAs depicted in Table 2 are model outputs and are those parameters which create an impact or interaction among the inputs, are of great interest.

Table 2: Output responses of the direct compaction process model

Parameter	Description	Unit
$x50$	Particle size x50	μm
σ	Tensile strength (without lubrication)	MPa
$\sigma_{Lubr.}$	Tensile strength (including lubrication)	MPa
F_{break}	Tablet hardness	N
t_{10}	Dissolution time till 10wt% of solid drug in dissolution	s
t_{20}	Dissolution time till 20wt% of solid drug in dissolution	s
t_{40}	Dissolution time till 40wt% of solid drug in dissolution	s
t_{50}	Dissolution time till 50wt% of solid drug in dissolution	s
t_{60}	Dissolution time till 60wt% of solid drug in dissolution	s
t_{80}	Dissolution time till 80wt% of solid drug in dissolution	s
t_{90}	Dissolution time till 90wt% of solid drug in dissolution	s

The assumptions made for the different model parameters were rather based on prior-knowledge and experience than experimental data except for the dissolution kinetic. Further work could aim at achieving model-based control of a real plant which requires detailed knowledge, model understanding and a model validation. With models matching the dynamic trajectories of a real plant to higher degrees a foundation for process development and control could be established.

2.2. Development of hopper model

The storage, transport and processing of granular medias in bins, hoppers and silos is vital for many production processes in the pharmaceutical, chemical, agricultural and food industry. Hoppers of all sizes and shapes are used to store and convey powders in numerous industrial applications [44]. For instance, in the continuous processes in the pharmaceutical industry the intermediates are stored in hoppers to guarantee enough available mass for subsequent unit operations in case of out-of-specification events [12]. An example is the delivery of powders to a subsequent rotary tablet press for compression in the pharmaceutical industry [2].

Despite the fact that the mechanisms of material flow within hoppers are studied over a long period, the basic knowledge about the mechanical interactions of the granular media is still incomplete. Most of the studied powder discharge has focused on conical hoppers, wedge-shaped hoppers, axisymmetric and plane flow hoppers. Yet, pharmaceutical tablet presses often use eccentric hopper designs that do not fall into either of these categories [45].

In recent years, modern computational models have been increasingly used to predict granular flow during hopper charge and discharge. These models enable prediction of mass flow rates based on material and design parameters. Additionally, phenomena such as bridge formation and segregation can be analysed by engineering correlations based on experience or with discrete element method (DEM) simulations [46], [47].

The capability of tracking material throughout the process is necessary in the field of pharmaceutical engineering. Within the process flowsheet, a hopper model was set up allowing to simulate dead-time based on filling level and mass flow rate by assuming plug flow of material (without dispersive mixing). The material tracking is based on the filling level of compartments caused by the inlet and outlet stream used to extract quantitative information of particles along a pharmaceutical manufacturing process. This provides information regarding

the path and location of particles as they travel along a downstream process, such as described later on for a direct compaction flowsheet. The developed hopper model, allows material tracking within the process with a first-in-first-out model (FIFO) with variable dead-time.
The model is implemented in gProms which is a powerful numerical solver environment, but due to the nature of its numerical solver capabilities it is not suitable for discrete time interaction. The only way some sort of dead-time can occur within the standard gProms models, is through low-pass behaviour of higher order. In order to bypass this problem so called "tasks" are used, which allow the implementation of schedules to shift parameters by a calculated dead-time t_d. Figure 9 depicts the schedule with logical conditional queries which are necessary to run the model. An implemented schedule specifies logical conditions at which the hold-up of a compartment is filled or discharged and to detect changes in the inlet stream characteristic to shift the outlet mass fraction by a certain time.

To run the model, it is necessary to detect changes within the feed stream. Changes or variations bigger than a defined threshold of the mass fraction or the particle size distribution, lead to the utilization of a new active compartment within a given ring-buffer. Equation 23 describes the calculation of the variation ΔE depending on the difference of the mass fraction from the currently filled compartment c_i and the discharged compartment c_j.

$$\Delta E = |c_i - c_j| \qquad \text{(Eq. 23)}$$

For each of the utilized and active compartments the mass balance equation is solved. Within each compartment the information regarding the current hold-up, mass fraction and PSD is contained. In the described algorithm (detailed explanation in Figure 8), N represents the number of active compartments, j is the counter variable in the ring buffer of the discharged compartment and i the current compartment which is filled.

In general, three different cases can be distinguished, depending on the number of active compartments N. In case only one compartment is active ($N = 1$) the hold-up is affected by the inlet- and outlet mass flow rate. With two compartments active ($N = 2$) the upper one is filled and the bottom compartment discharged.
If the number of utilized compartments is greater or equal to three ($N \geq 3$), it is similar to the two compartments case, with the difference that the hold-up of all the compartments between the filled and discharged compartments stay constant ($\frac{dm_{HU,j+1:j+N-2}}{dt} = 0$).

Table 3: ODE for different possible occurring compartment cases.

Number of compartments $N = 1$:	$\frac{dm_{HU,j}}{dt} = \dot{m}_{in} - \dot{m}_{out}$ $\frac{dm_{HU \neq j}}{dt} = 0$
Number of compartments $N = 2$:	$\frac{dm_{HU,j+1}}{dt} = \dot{m}_{in}$ $\frac{dm_{HU,j}}{dt} = -\dot{m}_{out}$
Number of compartments $N \geq 3$:	$\frac{dm_{HU,j+N-\mathrm{i}}}{dt} = \dot{m}_{in}$ $\frac{dm_{HU,j+1:j+N-2}}{dt} = 0$ $\frac{dm_{HU,j}}{dt} = -\dot{m}_{out}$

The three different cases are explained in Table 3 and outlined in Figure 8. It can be noticed that the delay of the outlet stream characteristics is depending on the hold-up of the hopper compartments and can be characterized by: $c_{out} = c_{in,j+N-1}$.

As seen for compartment 1, hold-up is building up and the compartment is filled and discharged at the same time ($N = 1$, $\frac{dHU_1}{dt} = \dot{m}_{in} - \dot{m}_{out}$). This happens till a change in the inlet mass fraction occurs so that two compartments become active. With more than one compartment active, one is filled and the previous one is discharged at the same time ($N = 2$, $\frac{dHU_1}{dt} = -\dot{m}_{out}$, $\frac{dHU_2}{dt} = \dot{m}_{in}$). In case compartment 1 is empty and no new change causes utilization of a new compartment, $N = 1$ again and the hold-up of compartment 2 increases with $\frac{dHU_2}{dt} = \dot{m}_{in} - \dot{m}_{out}$ until the inlet stream characteristics change.

Since the hold-up of compartment 2 is relatively large and based on the assumptions that the mass flow rates stay constant over time, it takes relatively long to discharge compartment 2. This can also be noticed by the time delay in the outlet mass fraction. In the meantime, several fluctuations in the inlet characteristic occur leading to the case where $N = 3$ for compartment 4. Due to the fact that compartment 2 is still discharging, the hold-up of compartment 3 is constant.

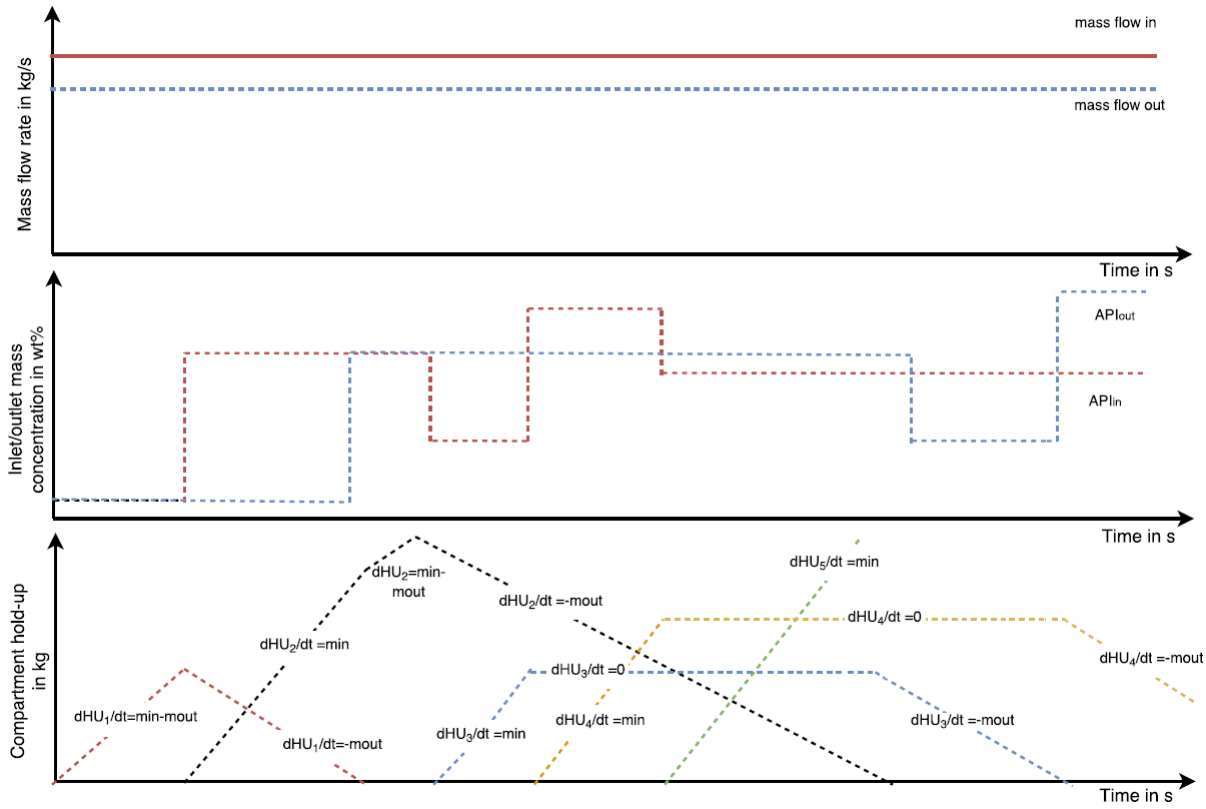

Figure 8: Illustrative example of the basic implementation principle. The figure depicts the mass balance equation of each compartment. Both, the larger inlet and outlet mass flows are constant over time. Each time a characteristic in the inlet stream changes, a new compartment is created.

Figure 9 describes the procedure within the main task of the simulation in detail. The queries are sequentially processed in a certain and necessary order. A changing inlet characteristic is saved temporarily and assigned to the outlet stream depending on whether a new compartment is discharged. We are assuming that the mass fraction entering the hopper first is the mass fraction that is leaving the hopper first in a FIFO order. It is known that the usage of a FIFO model does not simulate the real-world behaviour of a hopper. But since the real behaviour of powder flow within a hopper is strongly material and hopper design correlated and not yet fully understood these simplification and assumptions seem to be reasonable. The model implementation is based on several assumptions. Within the hopper compartments, no mixing of the phases or the components can occur. Furthermore, no reaction of material takes place.

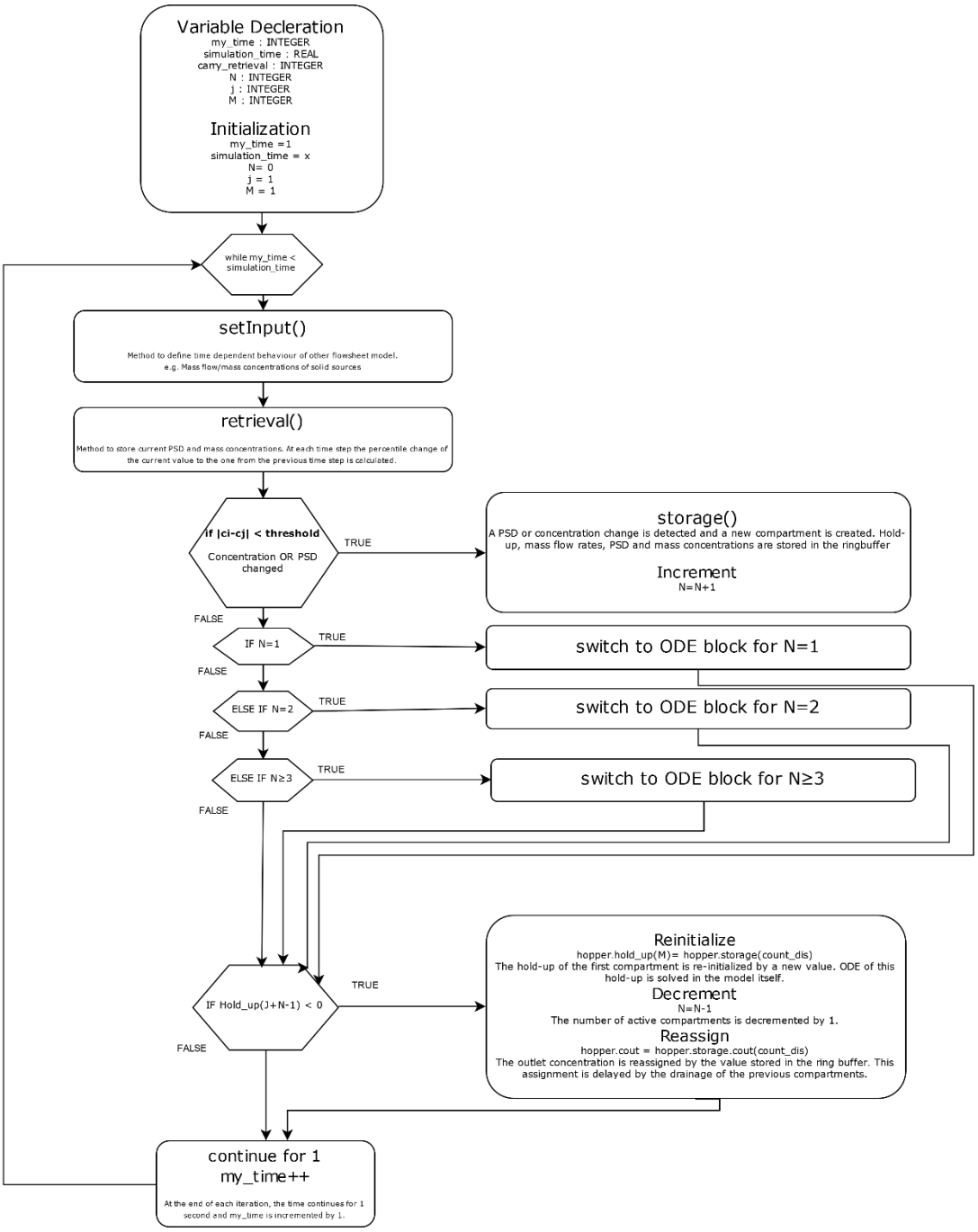

Figure 9: Flow diagram of the schedule implementation in the newly developed custom hopper model.

Due to the discrete time steps of 1s, a change within the inlet stream is recognised by a time delay of 1s according to the specified time step of the iteration. Figure 19 shows the effect at second 20, where the outlet mass fraction c_{out} is offset by 1 second.

gProms creates several values for the same time step (each reassignment within a task creates an additional value for the same time step). Despite the fact that the values at a time step are always the same it affects the size of the simulation file. It is possible to highly enhance simulation performance by using the Monitor on/off function provided for gProms tasks. Due

to the usage of modulo operation and the application of the Monitor on/off function it is possible to monitor the simulation results at a certain time interval. This monitoring isn't affecting the simulation at all, but rather allows the user to save and load the results file faster since the number of sample points can be reduced, resulting in a smaller file size.

The selected resolution of the sampling interval is affecting the accuracy of the simulation outcome. As default, the sampling interval is set to $1s$, meaning that a task is only performed once every second. The simulation is iterated until the final simulation time is reached. Despite that, the numerical integration of the ODE's of the model is not affected.

Increasing the sampling time leads to a decrease in the percentile error between the hold-up calculated by the ODE (equation 24) and the hold-up calculated by the sum of all compartments (equation 25).

$$\frac{\boldsymbol{dHU}}{\boldsymbol{dt}} = \dot{\boldsymbol{m}}_{\boldsymbol{in}} - \dot{\boldsymbol{m}}_{\boldsymbol{out}} \qquad \text{(Eq. 24)}$$

$$HU = \sum_{i=1}^{N} HU_i \qquad \text{(Eq. 25)}$$

The numerical error of the accumulated hold-up is depicted in Figure 10 and shows how this sort of resolution is affecting the model outcome. It illustrates the problem very well at second 56 and 91 where the compartment hold-up is negative for a very short period of time. This is caused by the if statement, which is checked during sampling whether the hold-up of the discharged compartment is below zero. Nevertheless, the hold-up of the compartment could already be beneath zero, leading to a numerical offset.

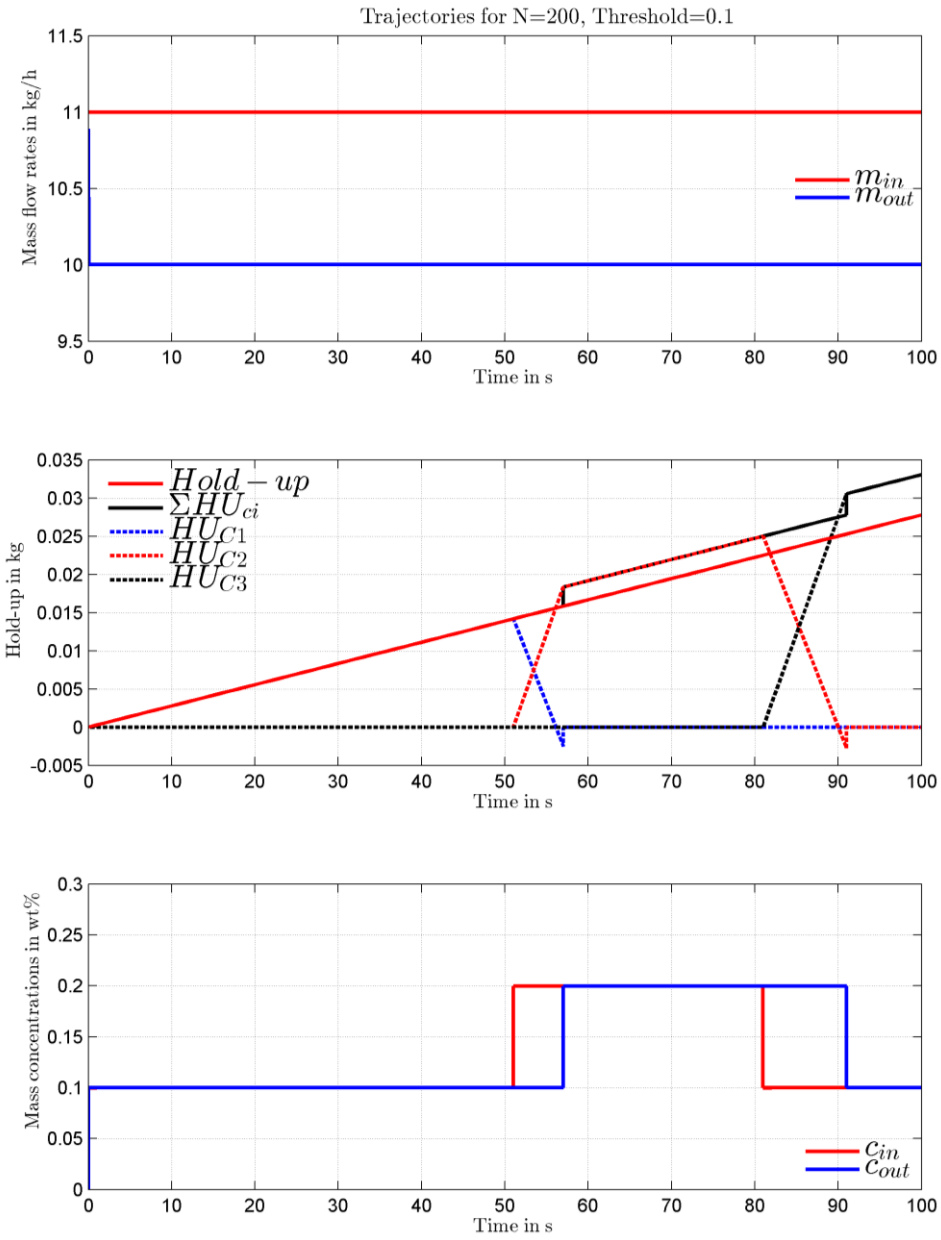

Figure 10: Comparison between the hold-up calculated with the ODE and the hold-up calculated by the sum of each compartment mass. Figure illustrates the filling of three compartments.

The number of possible compartments respectively the size of the ring buffer is clearly affecting the simulation time since it requires more differential equations being solved. Because of that, the model is implemented with a fixed size ring buffer. In case the number of active compartments is larger than the number of empty ones, an error message is displayed in the execution output. In this case the ring-buffer has to be set to a larger value to avoid an overflow of active compartments.

The dialog for the hopper model is shown in Figure 11 where the outlet mass flowrate of the hopper can be specified directly by the user. This tab is also used to provide specifications related to the operation of the hopper and to specify the initial conditions of the hopper in case the hopper is pre-filled at the start of the simulation. Initial parameters include the particle size distribution, mass fraction and the mass.

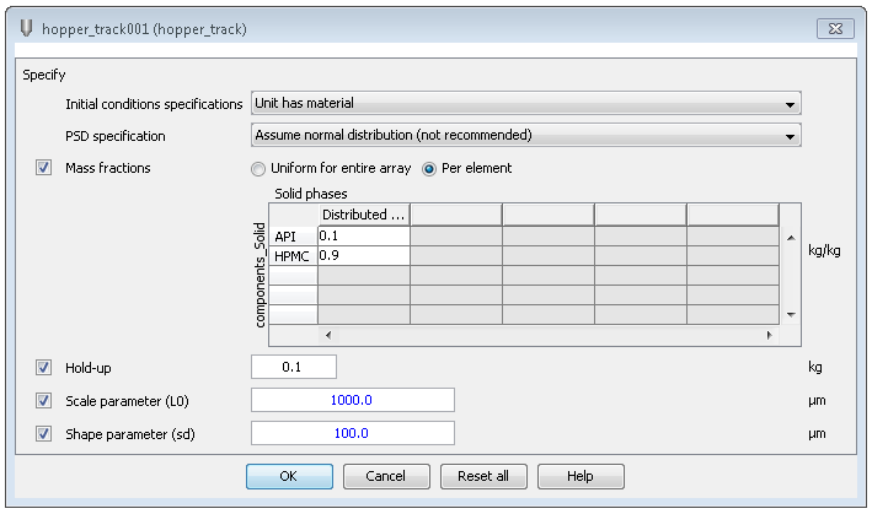

Figure 11: The custom hopper model dialog with the configuration window.

2.3.Blender

The blender model is describing the transport of material through a continuous horizontal blender via a plug-flow description. The mass balance equations are well described in [48] and are not considered influential for this examination. The rate of change of any given species in phase p at any given point z of the unit is given by:

$$\frac{\partial C_{i,p}(z)}{\partial t} + \frac{u}{L}\frac{\partial C_{i,p}(z)}{\partial z} = \frac{D_p}{L^2}\frac{\partial^2 C_{i,p}(z)}{\partial z^2} \quad \forall i \in I, \forall\, p \in P, \forall\, z \in]0,1[\tag{Eq. 26}$$

With $C_{i,p}$ being the mass concentration of species i in phase p in $[kg/m^3]$, u the velocity of material within the unit in $[m/s]$, L the length of the unit $[m]$, D_p the dispersion coefficient in phase p in $[m^2/s]$, I a set of species in the system and P set of phases in the system.

The mass flow rate into the unit u is giving the material a velocity as following:

$$u = \sum_{j=1}^{N_{inlet}} \sum_{p \epsilon P} \frac{F_{j,p}^{in}}{\rho_{j,p}^{in} \cdot A_{cross}} \tag{Eq. 27}$$

With $\rho_{j,p}^{in}$ being the density of phase p in the j[th] feed stream in $[kg/m^3]$ and A_{cross} the cross sectional area of the hopper unit in $[m^2]$.

2.3.1. Lubrication

Lubrication refers to the addition of lubricants during powder blending or mixing operations. The extent of lubrication K relates to the amount of shear strain on powders and can be calculated with equation 28 for continuous operation.

$$K = \alpha \cdot v_{tip} \cdot \tau \tag{Eq. 28}$$

K is the extent of lubrication for continuous operation in $[dm]$, α is an empirical geometric parameter [-], v_{tip} is the tip speed in $[dm/s]$ and τ is the mean residence time $[s]$. The tip speed is related to the rotation rate and the agitator diameter specified in the model.

2.4. Feed frame

The model describes the transport of material through a feed frame to the tablet press via plug flow. The operation of the tablet press determines the mass flow rate out of the feed frame. This model can be treated as another blending unit and is using a similar modelling approach.

2.5. Tablet press

A tablet press is a mechanical unit operation that compresses blends of powder into tablets of uniform size and weight. The compression force on the powder can be linked to the porosity of the produced tablets, which is a significant quality attribute of the end-product. The model equations describe relatively basic and capture key physics typically observed experimentally, namely: the porosity of the tablet, tensile strength and the breaking force of the tablet.

2.5.1. Tablet porosity

The compaction force F_{comp} $[N]$, experienced by the tablets is related to the applied compaction pressure P_{comp} $[Pa]$ and the cross section area of the tablet A $[m^2]$ as follows:

$$P_{comp} = \frac{F_{comp}}{\pi \cdot A} \quad \text{(Eq. 29)}$$

The change in relative density of the tablet is related to the applied compaction pressure via the compressibility constant as shown below.

$$RD_{tablet} = RD_{initial}(P)^{1/K} \quad \text{(Eq. 30)}$$

With RD_{tablet} being the final relative density of the tablet after compaction [-], $RD_{initial}$ the initial relative density of the material in the tablet [-] and K being the compressibility constant in [-].

The relative density is the ratio of the bulk density to the skeletal density where the skeletal density corresponds to the crystalline density of the material in the tablet.

$$RD_{initial} = \frac{\rho_{bulk,initial}}{\rho_{skeletal}} \quad \text{(Eq. 31)}$$

$$RD_{tablet} = \frac{\rho_{bulk,tablet}}{\rho_{skeletal}} \quad \text{(Eq. 32)}$$

The porosity of the tablet is related to the relative density of the tablet by the following linear relationship.

$$\epsilon_{initial} = 1 - RD_{initial} \quad \text{(Eq. 33)}$$

$$\epsilon_{tablet} = 1 - RD_{tablet} \quad \text{(Eq. 34)}$$

$\epsilon_{initial}$ is the initial porosity of the material before compaction [-], ϵ_{tablet} is the porosity of the tablet after compaction [-].

2.5.2. Tensile strength

If the tablet is made by direct compression of the initial blend, the tablet tensile strength σ is obtained by the Ryshkewitch-Duckworth equation.

$$\sigma = \sigma_{mixture} e^{-k_{mixture}\epsilon} \quad \text{(Eq. 35)}$$

With $\sigma_{mixture}$ being the tensile strength of the solid mixture in the absence of porosity [Pa], $k_{mixture}$ being the bonding capacity of the solid mixture [-]. The authors suggest that volumetric mixing rules should be used to obtain the mixture tensile strength and bonding capacity as shown below.

$$k_{mixture} = \sum_{i \epsilon S} x_{vol,i} \cdot k_i \quad \text{(Eq. 36)}$$

$$\sigma_{mixture} = \sum_{i \epsilon S} x_{vol,i} \cdot \sigma_i \quad \text{(Eq. 37)}$$

$x_{vol,i}$ is the bulk volume fraction of species in in the material in the tablet [-], k_i is the pure component bonding capacity of species i [-], σ_i is the pure component tensile strength in the absence of porosity [Pa], S is the set of chemical components in the material of the tablet.

2.5.3. Tensile strength (including effect of lubrication)

With lubricants added to the mixture it is possible to adjust product quality attributes including tensile strength, disintegration and dissolution times. As seen in equation 38, the effect of lubrication leads to decrease in tablet tensile strength σ_{Lub}.

$$\sigma_{Lub} = \sigma \ (\beta \cdot e^{-\gamma K_{tot}} + 1 - \beta) \quad \text{(Eq. 38)}$$

With K_{tot} being the cumulative extent of lubrication (calculated from upstream mixing unit operations) in [-], β and γ are material specific parameters [-] and σ being the tablet tensile strength (unlubricated) in [Pa].

2.5.4. Breaking force

The breaking force which is the force required to break a tablet into its constitute material is related to the tablets shape and overall tensile strength. For round flat face tablets this can be calculated from the breaking force according to equation 39.

$$F_{break} = \frac{\pi D t}{2} \sigma \quad \text{(Eq. 39)}$$

With σ is the tensile fracture strength of the tablet $[Pa]$, F_{break} is the fracture force $[N]$, t is the overall thickness $[m]$ and D is the tablet diameter $[m]$.

2.6. Dissolution model

The in vitro vessel model is a generic vessel model which can be used to build in vitro dissolution and precipitation experiments. The subsequent equations touch upon the implementation of the dissolution model [49]. The tablet mass in the liquid medium at any given point in time is assumed to be governed by the following differential equation.

$$\frac{dm_{tablet}}{dt} = -k_{dis} \quad \text{(Eq. 40)}$$

where m_{tablet} is the total mass per tablet in the system $[kg]$, and k_{dis} is the disintegration rate constant per tablet $[\frac{kg}{s}]$.

2.6.1. Modified release

In the equation below, the disintegration rate is assumed to be related to the tablet porosity.

$$R = k \cdot m \cdot e^{\alpha \cdot \epsilon} \quad \text{(Eq. 41)}$$

Equation 41 describes the rate of disintegration on a mass basis of the composite phase by an empirical rate expression. R is the mass disintegration rate in $[kg/s]$, k being the rate coefficient in $[s^{-1}]$, the mass of the disintegrating phase in the system m in kg, the internal porosity of the disintegrating phase ϵ [-] and an empirical exponent α describing the porosity dependence [-]. With adequate experimental data of the dissolution profile and an in-vitro dissolution model describing the release profile, it is possible to estimate the model parameters to match the

experimental data. The more accurate reaction kinetic parameters are, the closer the model response is to reality.

The content of the composite is carried from upstream processes and is affected by the size distribution, composition, porosity and other factors captured, based on their values when the composite phase was formed. For the disintegrating composite it is assumed that the nested phases emerge with properties based on these upstream process variables. The upstream processes are described by the previous models equations.

2.6.2. Population balance equation

A population balance on particles of a given solid phase in the bulk liquid medium considers the rate of dissolution of the particles as well the rate of addition of particles to the liquid phase by disintegration of the tablets in the system.

$$V\frac{\partial[N_i(L)]}{\partial t} - V\frac{\partial[G_i(L),N_i(L)]}{\partial L} = k_{dis}\cdot n_{Tablet}\cdot N_{pt,i}(N) \qquad i \epsilon P, [L_{min}, L_{max}) \qquad \text{(Eq. 42)}$$

where V is the volume of the system [m^3], L is the size of the particle being considered [m], $Ni(L)$ is the number concentration density of particles of size L in solid phase i suspended in the liquid [# of particles/m3], $Gi(L)$ is the dissolution rate of particles of size L in solid phase i [m/s], n_{tablet} is the number of tablets in the system [# of tablets], $Npt,i(L)$ is the number concentration density of particles of size L in solid phase i in the tablet [# of particles/m³], P is the set of solid phases considered, L_{min} is the lower boundary of the particle size distribution domain and L_{max} is the upper boundary of the particle size distribution domain [50].

2.6.3. Dissolution

The dissolution process results in solid species being added to this surface at a rate of $\emptyset^{"}_{diff,i}$ in [$mol\, m^{-2}s^{-1}$]. Individual molar flux balances on particle surfaces are written for species in the liquid phase, including full chemical equilibria at the solid-liquid interface. The flux leaving the solid-liquid interface due to diffusion into the bulk is calculated for each species in the liquid phase as follows:

$$\emptyset^{"}_{diff,i} = \frac{D_i}{h_{UWL}}\left(C_i^s - C_i^b\right) \qquad \text{(Eq. 43)}$$

Where D_i is the diffusion coefficient in $[m^2/s]$, h_{UWL} is the thickness of the unstirred water layer around the solid in $[m]$, C_i^s is the molar concentration at the solid-liquid interface $[mol/m^3]$ and C_i^b is the bulk aqueous molar concentration in $[mol/m^3]$.

The boundary layer thickness is calculated from the particle characteristic length and the Sherwood number. If the calculated boundary layer thickness exceeds 30 µm, it is set to 30 µm, based on the work of Hintz-Johnson.

$$h_{UWL} = \frac{L}{SH} \quad \text{(Eq. 44)}$$

L is the particle characteristic length in $[\mu m]$, SH is the dimensionless Sherwood number. For non-dissociating solids (e.g. freeform), it is assumed that the concentration of the species at the solid-liquid interface is equal to its intrinsic solubility.

$$C_i^s = \frac{C_{sat}}{MW} \quad \text{(Eq. 45)}$$

With C_{sat} being the intrinsic solubility in $[kg/m^3]$ and MW being the molecular weight in $[kg/m^3]$. For a dissociating solid phase (e.g. a salt), it is assumed that the product of the concentration at the solid-liquid interface of the species composing the solid is equal to the salt solubility product.

3. Results

3.1. Hopper model test cases

In order to ensure that the model works sufficient, basically three different test cases are introduced. These described test cases define input specifications, execution conditions and testing procedures to verify that the hopper model is functioning as proposed.

3.1.1. Set-point changes

Often it is of great interest to see how a system responds to changes of the set-point. Set-point changes could be used to return a system to its norm. Such a set-point change could occur by upstream feeders changing the composition of the stream to take counter measures preventing OOS in another unit operation. As seen from the plots in Figure 14, the accumulated hold-up is clearly affecting the dead-time at which the inlet mass fraction is send to the outlet mass fraction. The comparison between the two plots shows that an increasing inlet mass flow rate results in a larger hold-up leading to a larger time delay within the outlet mass fraction.

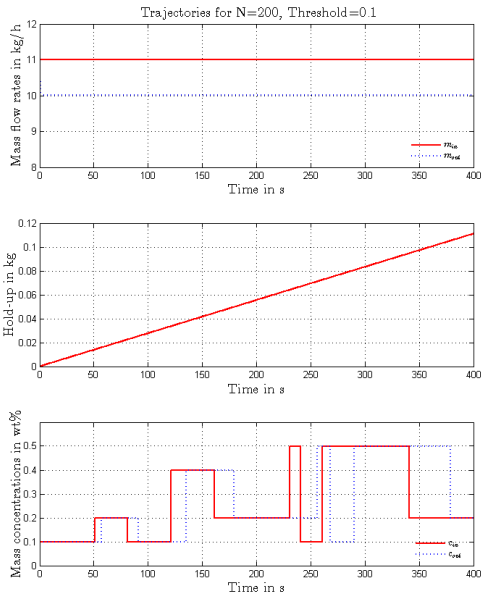

Figure 12a: Inlet mass flow rate at 11 kg/h.

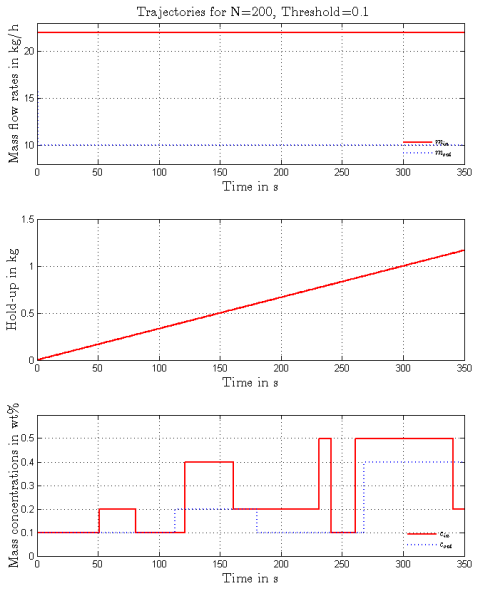

Figure 13a: Inlet mass flow rate at 22kg/h.

Figure 14: Trajectories from flowsheet simulation. Set-point changes of the mass fraction within the inlet stream and the resulting outlet mass fraction. The inlet and outlet mass flow rates stayed constant over time with a higher HU clearly affecting the time delay of the mass fraction in the outlet feed.

3.1.2. Linear ramp

Figure 15 depicts the distortion of the outlet mass fraction in case of a linear increase of mass fraction within the inlet stream. To address the issue whether the mass fraction in the inlet has changed, the inlet mass fraction is linearly ramped from 0 to 1wt% for a solid component (Figure 15). Since a feed change is only detected using equation 23, a constant slope of a linear ramp can only be detected in case its slope is below a user defined threshold.

Figure 16 is depicting a case where the hopper is initially filled and hold-up is building up, since more material is entering the hopper than leaving. With mass flow rates constant over time ($\frac{\partial \dot{m}_{in}}{\partial t} = \frac{\partial \dot{m}_{out}}{\partial t} = 0, \dot{m}_{in} > \dot{m}_{out}$) the resulting outlet mass fraction is also linear with a different slope caused by the constant time delay.

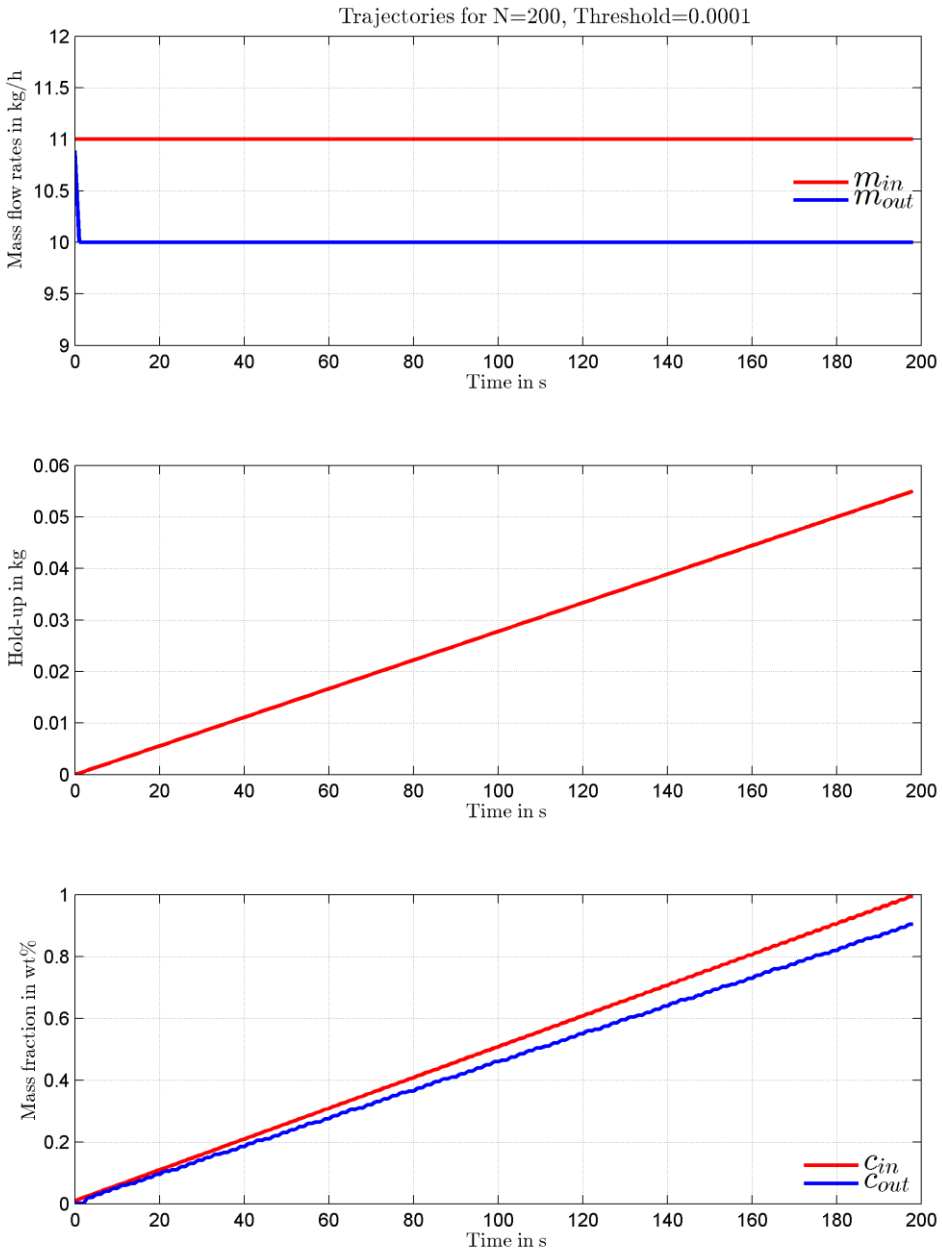

Figure 15: Trajectories from flowsheet simulation. Linear increase of the mass fraction of a single component within the inlet stream and the resulting outlet mass fraction. The inlet and outlet mass flow rates remain constant.

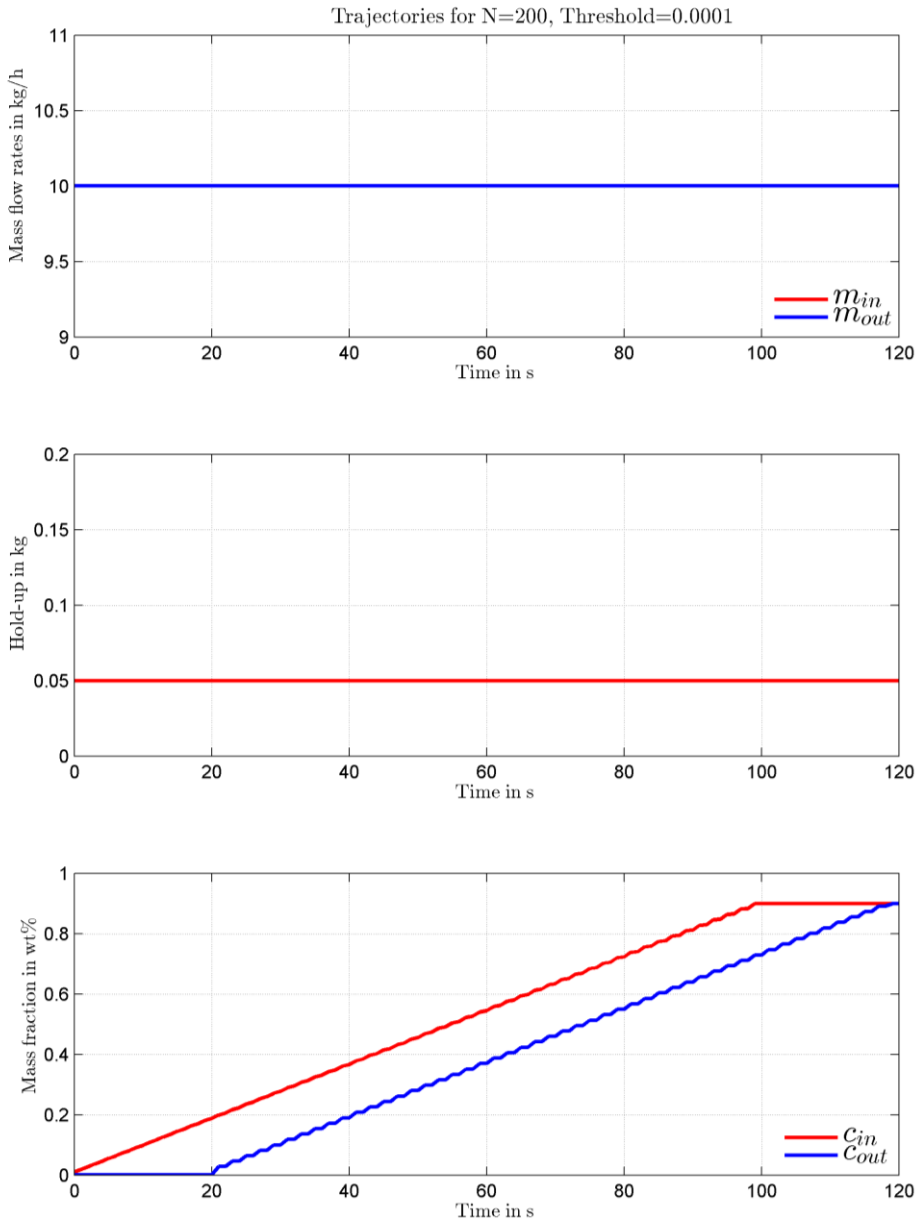

Figure 16: Hopper model is assigned with an initial hold-up. Due to the initial hold-up the outlet mass fraction is delayed by the time it takes to discharge the first compartment.

3.1.3. Sinusoidal trajectory

Figure 17 shows the trajectories for a sinusoidal mass fraction change at the hopper inlet. This conducted case demonstrates how the model performs during constantly changing compartment sizes.

This test case demonstrates that a sinusoidal input is leaving the outlet with a different frequency (considering a constant mass balance in each compartment). In this example, new compartments are utilized so fast (due to a permanent inlet change above the user defined threshold in mass fraction) that the period width of the outlet mass fraction is affected by filling and discharge of the hold-up in each compartment. During this specific case, all active compartments get the same hold-up and behave as all the other active compartments. Due to the increasing hold-up and the changing inlet mass fraction, the outlet mass fraction gets distorted by the duration it takes to discharge every single compartment.

The choppy trajectory of the outlet mass fraction seen in Figure 17 occurs due to the time it takes to empty the compartments. The time delay is caused by the sampling time and relates to the time it takes a compartment to get filled or discharged. Otherwise, a smaller threshold at which compartments are utilized in the ring buffer would lead to a greater number of active compartments with less compartment hold-up and a smoother trajectory.

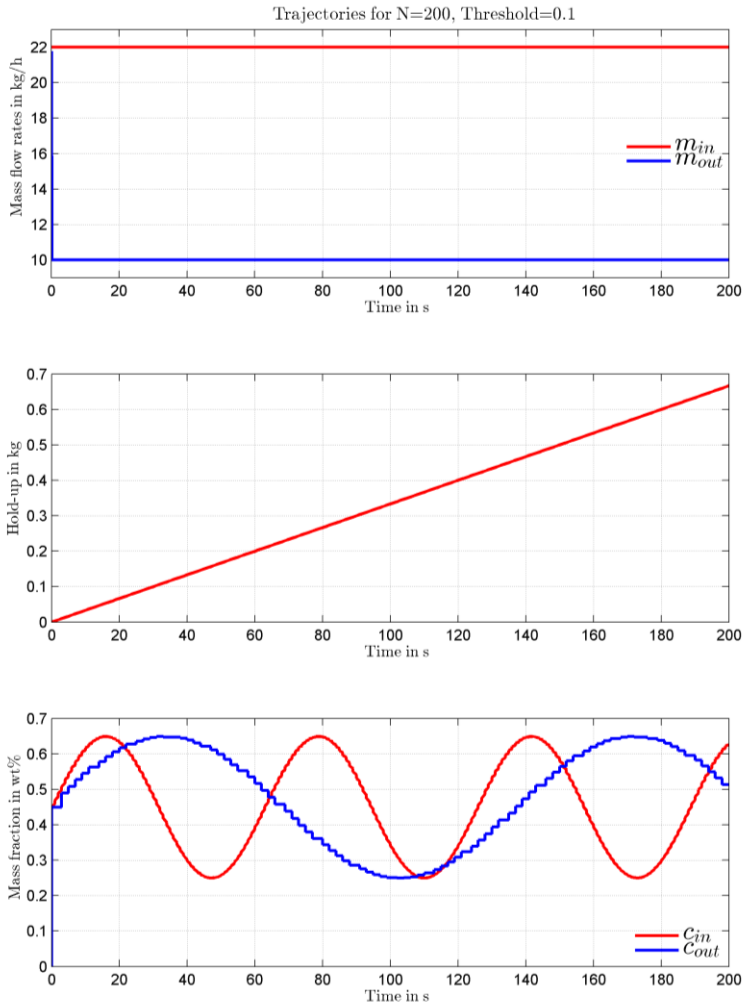

Figure 17: Trajectories from flowsheet simulation. Sinusoidal trajectory of the mass fraction within the inlet stream and the resulting outlet mass fraction. The inlet and outlet mass flow rates stayed constant.

3.1.4. Model application to a manufacturing process

A more sophisticated implementation of the hopper model is shown in Figure 18 where the hopper is affected by the output of several upstream unit operations. This example of a real-world application is showing a direct compaction line including two flaps, which are assuring that material which is out of specification (OOS) is discharged from the process. This flowsheet examines the behaviour of the plant during start-up until steady-state is reached. Due to material discharge from the upstream flap the resulting trajectories are depicting an interesting test case (Figure 19).

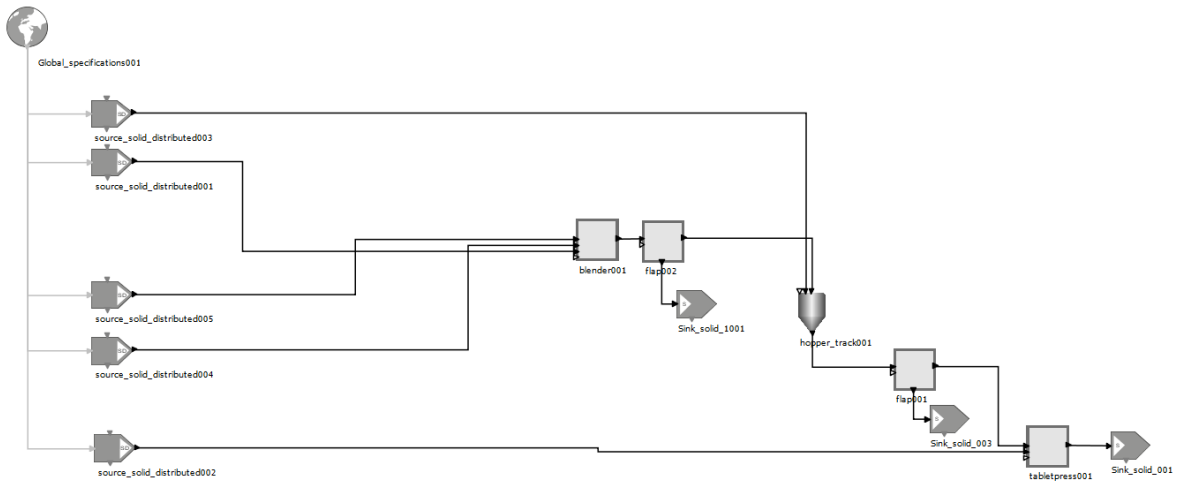

Figure 18: A sophisticated test case where the hopper model inlet stream is affected by several previous unit operations.

It can be observed that hold-up is building up and that the mass fraction is changing due to the initialisation of the upstream blender unit operation and the thereby increased mass flow rate. Almost straight from the beginning material is building up, until the initialisation of the blender is completed. The hopper hold-up is only decreasing during two periods where material is ejected by the upstream flap. Caused by an out of specification condition in the upstream process, a flap is discharging material from the process at second 210 and 610. The hopper inlet stream is therefore abruptly interrupted by the upstream flap. Due to the FIFO implementation of the hopper (described in Chapter 2.2.), the outlet mass fraction is clearly delayed by a time t_d only related to the hold-up and the outlet mass flow rate. The decline in the inlet mass fraction is delayed by 568s and can be calculated by equation 46.

$$t_d = HU/\dot{m}_{out} \qquad \text{(Eq. 46)}$$

With $\dot{m}_{out}$ being the outlet mass flow rate in $[kg/h]$ and HU the hopper hold-up in $[kg]$. Relating to the gain of the hopper hold-up (till 190s) and despite the fact that the inlet and the outlet mass fraction are set equal, a distortion in the hopper inlet caused by the OOS condition is absorbed and distorted over time.

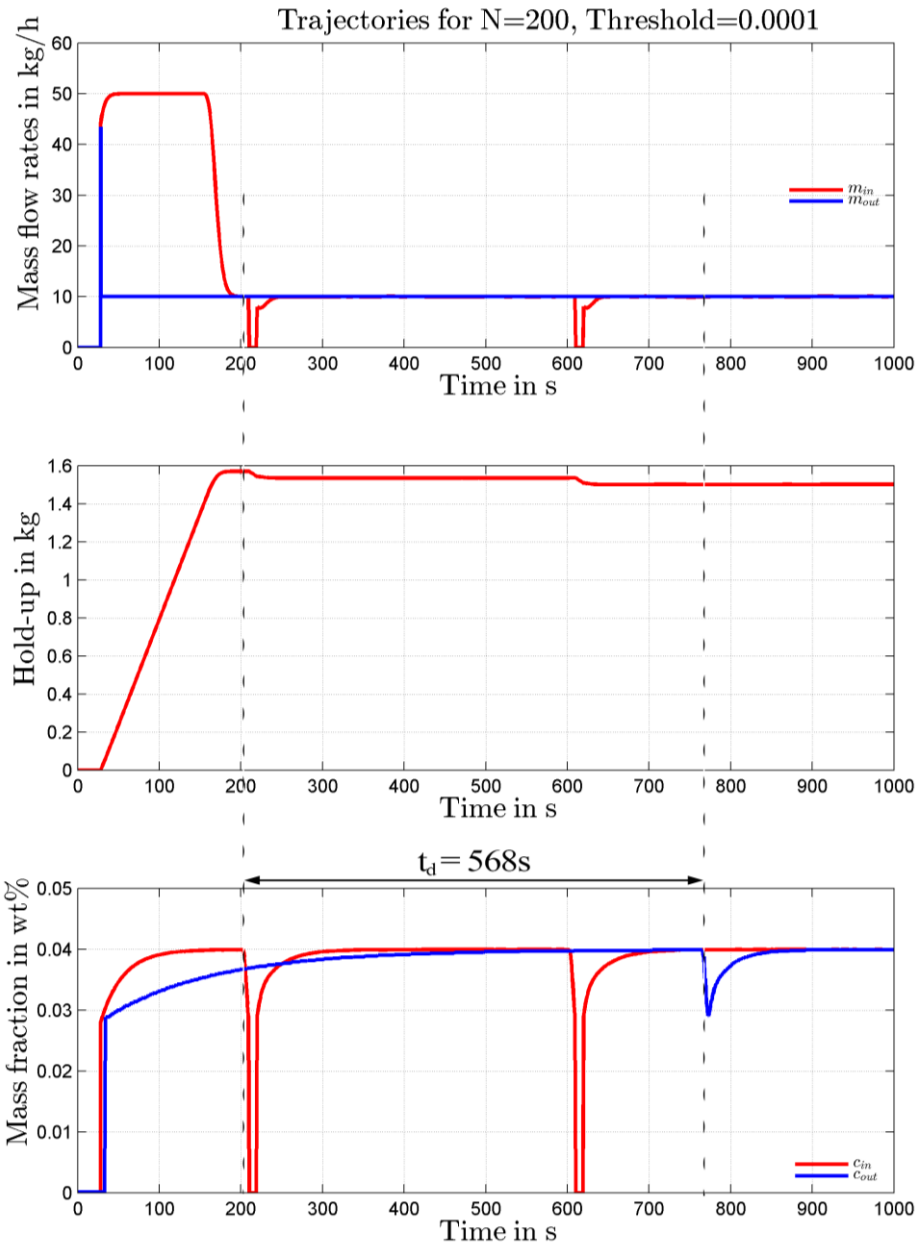

Figure 19: Case study with trajectories from a more complex flowsheet simulation. At second 220 and 600 the inlet mass flow is zero due to the fact that the upstream flap detected a mass flow which is out of specification and discharged the material from the production stream.

3.1.5. Performance enhancement

The accumulated discrepancy between the actual hold-up and the compartment hold-up is already described in Section 2.3. Caused by the simulation the resulting numerical error of the compartment hold-up is mainly depending on the sampling interval and the number of compartments.

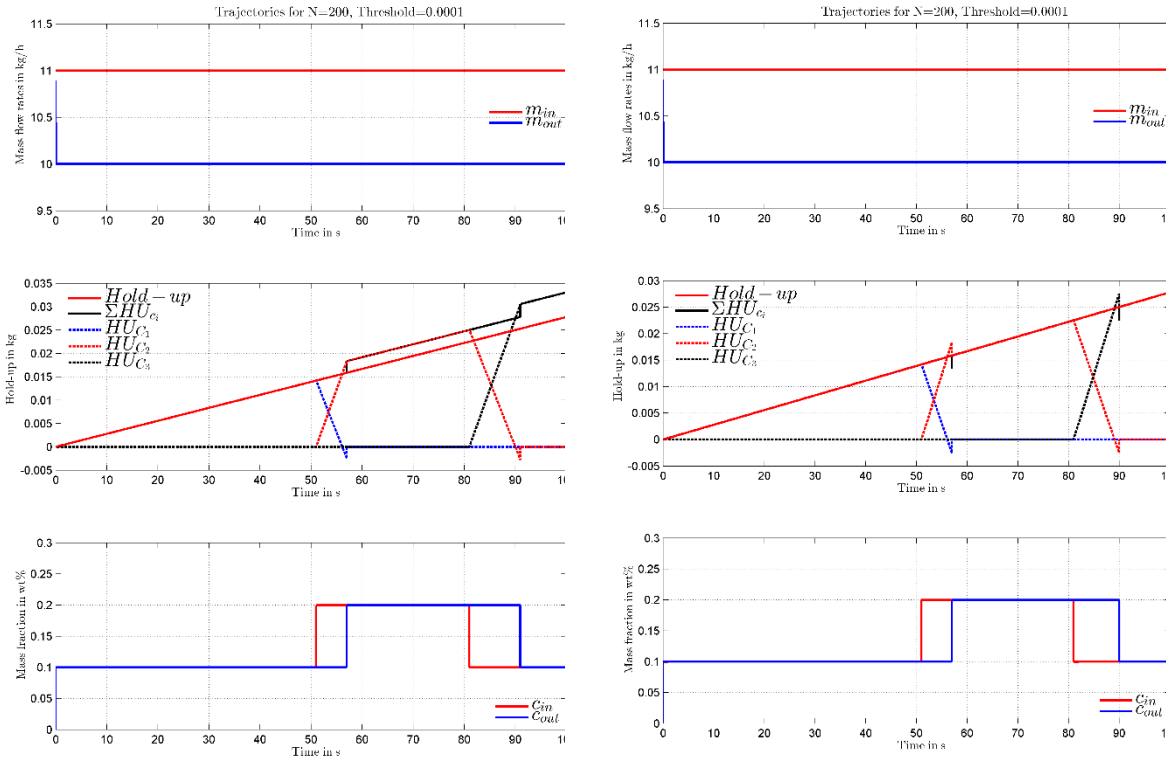

a) Numerical error accumulates and causes problems regarding the dead time.

b) Numerical error is resolved by reinitializing the compartment hold-up.

Figure 20: Comparison between the hold-up calculated with the ODE and the hold-up calculated by the sum of each compartment mass. Figure illustrates the filling of three compartments.

To remove the numerical error shown in Figure 20 a), it is necessary to subtract the resulting difference between the two hold-ups from a compartment each time the compartment hold-up reaches zero. Decreasing the sampling interval is reducing the effect of the numerical error since a correction happens more often. Nevertheless, this is leading to a higher computational demand and therefore a longer simulation time of the overall flowsheet. This is a disadvantage since the sampling interval is affecting every model in a flowsheet simulation and causes more computational costs, not only for the hopper model. On the other hand, by reducing the threshold at which a compartment is utilized the shape of the outlet trajectory is affected. A

lower threshold could not necessarily lead to more compartments (depending on the input trajectories) and is affecting the time lag at which material is leaving the hopper.

Caused by the fact that the ring buffer size is affecting the computational time as well, a number of simulations were performed to estimate the computational costs. Table 4 depicts the computational time it takes to run the hopper model for different number compartments and thresholds. The nine conducted simulations showed clearly that a higher compartment number and a smaller threshold lead to a longer simulation time. This is especially relevant for longer lasting flowsheet simulations with dynamic behaviour, where the process time could last several minutes. More complex flowsheets with several unit operations and re-cycles tend to take longer to reach a steady-state.

Table 4: Simulation time of the hopper model for different ring buffer sizes $\boldsymbol{M}$ (max. number of possible compartments) and the threshold.

	Threshold for inlet stream		
Ring buffer size *M*	0.0001	0.00505	0.01
M=50	36s	37s	27s
M=175	87s	70s	58s
M=300	170s	137s	95 s

3.2. Comparison to hopper model from standard library

The model developed by PSE (Process Systems Enterprise Ltd.) is used to dynamically model transportation and storage of material. The hopper geometry is approximated as a cylinder placed on top of an inverted truncated cone. In a typical flowsheet the hopper is used as a storage vessel and is connected to a source and two sinks. One sink connected to the hopper bottom and one for the overflow (Figure 21).

Depending on the specified geometry of the hopper it has a maximum storage capacity. Material exceeding the upper fill level is removed via the overflow stream. The model relies on a few basic assumptions. Multiple solid streams are instantaneously mixed before the first-in/first-out procedure applies to the stream. For each phase separate energy, mass and population balances are considered. During the time material is in the hopper, no breakage, agglomeration, drying, wetting or other transformative event takes place. No transfer of heat between the unit to its environment and among the phases is considered during the calculation. The user has to choose whether the outlet mass flow rate is specified or calculated by mechanistic relationships with key equations well documented in [51].

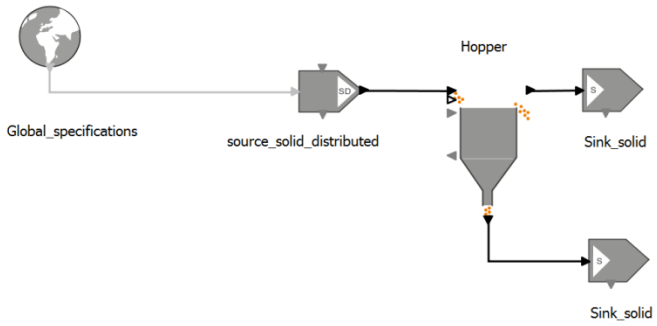

Figure 21: A simple flowsheet including a hopper model. Material attributes are assigned in the Global specifications and the solid source.

Due to the standard models incapability of model-based material tracking, the development of a custom hopper model was required. Another reason for developing a new model was the fact that the hopper model from PSE takes longer to simulate depending on the specified number of axial size bins. To fit the need for material tracking, a FIFO based model was developed where the delay of the outlet stream characteristics was hold-up depended.

3.3. Sobol Indices

With Sobol's indices the first and total-order effects are quantifying, how the variation in the input parameters is contributing to a variation in the output. One reason why total Sobol' indices are interesting is interaction. The inputs are interacting when their joint effect on the output is different from the sum of their individual effects. Another advantage of using Sobol indices is the possibility of applying them to linear and non-linear models. They deliver the impact of variables independent of the assumption of a linear relationship.
It was investigated if the input factor i.e. μ_{API} is involved in interactions with other input factors. The difference between $S_{Ti}-S_i$, is a measure of interaction between a given factor X_i and all the other factors. Highlighting these interactions among variables helps to improve the understanding of the model structure. However, they provide no information to tendency and the absolute value of the correlation. It is important to estimate these parameters to the highest accuracy due to their main effect.

Several publications mention the importance of proper visualization of the sensitivities for a better and intuitive understanding of the results. Visualization capabilities are key for a successful application of sensitivity analysis since a complex behavior can be mapped in a simple and more intuitive manner [52]. Therefore, Figure 22 and Figure 23 are showing the first and total-order indices of 5200 model runs, presenting the sensitivity indices in a color coded way. On the y-axis are the 6 input parameters (as described in Chapter 2.2.1.) with 10 corresponding model outputs on the x-axis. Trying to specify a larger amount of factors would require a large number of evaluations and excessive CPU time. The total CPU time is dependent on size and complexity of the flowsheet model, number and range of factors and the sensitivity analysis method. Therefore, it is favorable starting at a small sample size (as investigated in Chapter 3.3.1.) and increase the number of samples for the analysis as needed. Due to the computational costs it is recommended to keep the number of simulations to a reasonable minimum. To check whether an appropriate number of samples is being used, it is necessary to check for convergence of the calculated Sobol indices. Based on the convergence of the output factors, a sufficient sample size of 5200 could be found as discussed in Chapter 3.3.1.

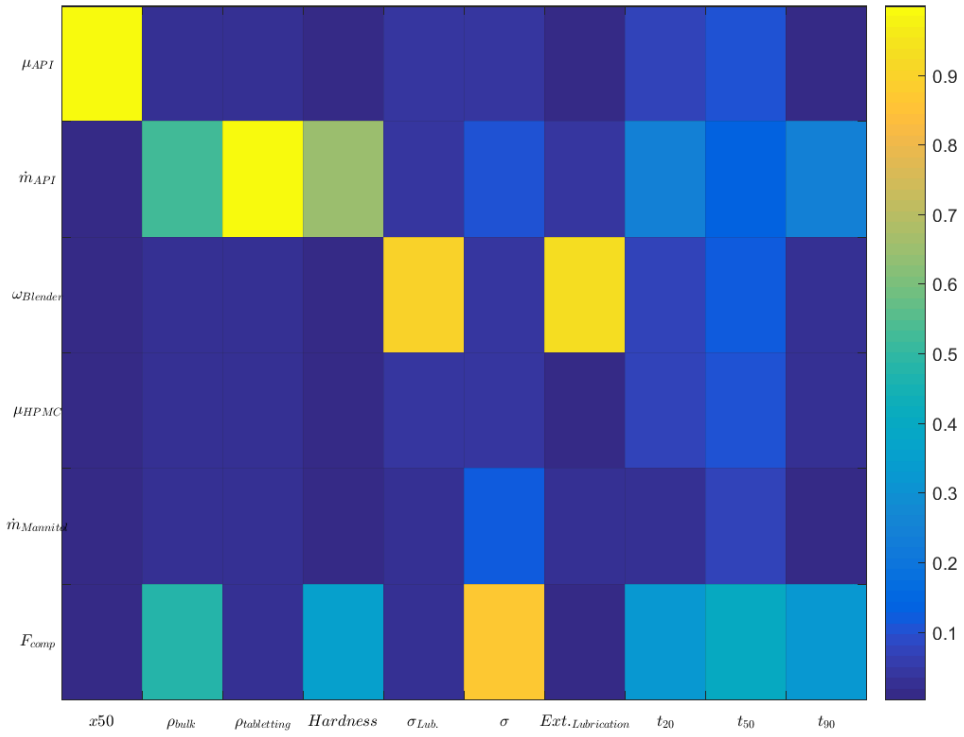

Figure 22: Simulation results of the Sobol first-order indices (5200 model evaluations). The intensity plot shows the first-order indices of the input variation on all of the output variables. The greater the sensitivity indices the more critical become the parameters affecting the output variability.

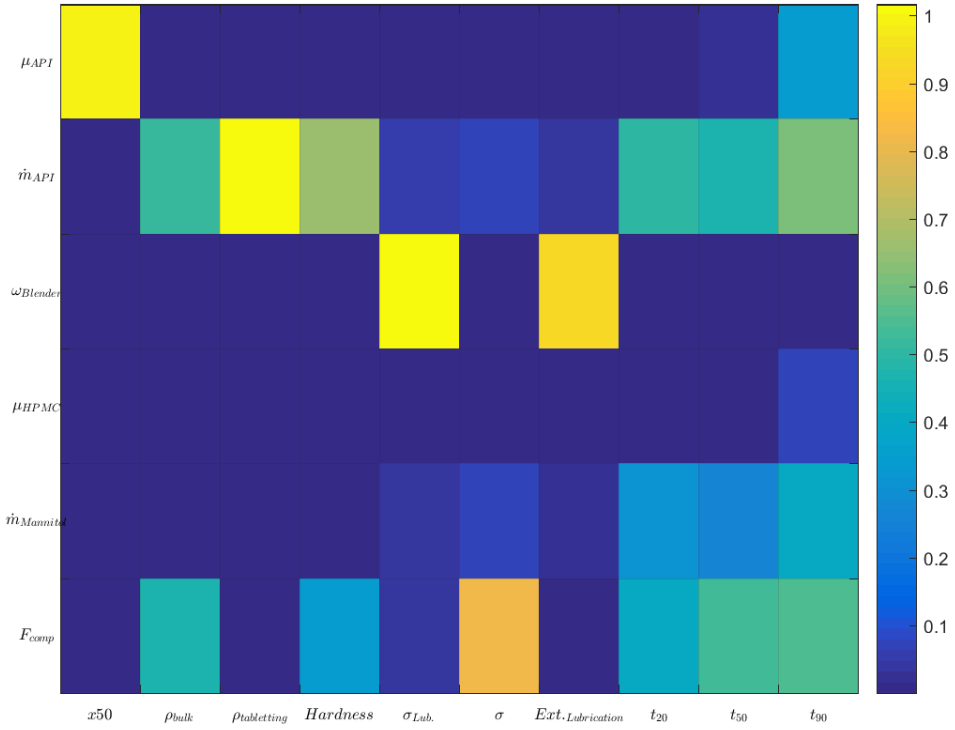

Figure 23: Simulation results of the Sobol total-order indices (5200 model evaluations). The intensity plot shows the total-order indices of the input variation on all of the output variables. The greater the sensitivity indices the more critical become the parameters affecting the output variability.

The negative signs in Figure 22 are due to numerical errors in the Sobol' indices. Using the Sobol method such negative values could be encountered when the analytical sensitivity indices are close to zero (i.e. this relates to not affecting or unimportant factors). As described in the subsequent chapter, increasing the sample size of the analysis reduces the probability of having negative indices.

Tablet porosity and tablet hardness: It can be concluded that the tuning of API particle size distribution, as its effect on the uncertainty on the tablet hardness and porosity is negligible. The particle size distribution of the API μ_{API} seems to be not affecting the porosity or tablet hardness. This can be caused by the small mass fraction of API in the formulation and the high solubility of the API in the solvent.

Tensile strength: Figure 23 depicts the tensile strength for two different calculations. One with the tensile strength affected by lubrication σ_{Lub} and once without (σ). It is clearly noticeable

that σ_{Lub} is affected by the rotation rate of the blender which clearly relates to equation 38. The tensile strength σ (equation 35) on the other hand is basically the base for the calculation of σ_{Lub} and is mainly affected by F_{comp}.

Breaking force: The uncertainty in $\dot{m}_{API}$ and the compaction force are the main contributors to the uncertainty in the output. The analysis revealed very little interaction when comparing the total sensitivity indices with the first order sensitivity indices. Considering the breaking force/tablet hardness this simply undermines the importance of $\dot{m}_{API}$ and F_{comp}. These are both controllable process parameters attributing differently to the overall mass fraction. One might be encouraged to carry out further analysis searching for the optimal value for these factors to reduce the uncertainty in the analysis outcome. Without GSA we would have accepted the fact that most of the uncertainty in the tablet hardness is due to intrinsic problem uncertainty and therefore unavoidable. The other factors shown in Figure 22 and Figure 23 are not considered as significant since their main contribution to the output is below 5%. The best expectable gain in terms of reduction of output variance is 60% obtained on average by learning about the effect of $\dot{m}_{API}$. In terms of factor prioritization this factor will reduce the output variance of the breaking force the most by setting it to a fixed value within its pre-defined range. With Sobol's indices it is possible to apportion the importance of an input factor with respect to a model output with a quantitative measure.

Dissolution profile: The sensitivity analysis regarding the dissolution profile was carried out by calculating the release of a drug substance from the dosage form, ranging from a minimum dissolution rate (t_{10}) to a maximum dissolution rate (t_{90}). The dissolution rate was recorded by incremental steps of 10wt% leading to corresponding dissolution times. Lakio et al. provide several dissolution data which laid the foundation for estimating the parameters of the release function [37]. They used an experimental set-up to estimate dissolution characteristics in such a way that the formulation composition, the material characteristics, as well as the operational settings were affecting factors. Figure 24 depicts the dissolution profile for input values set to their nominal values. The y-axis is showing the fraction of total API dosed dissolved with 100% relating to a completely dissolved component.

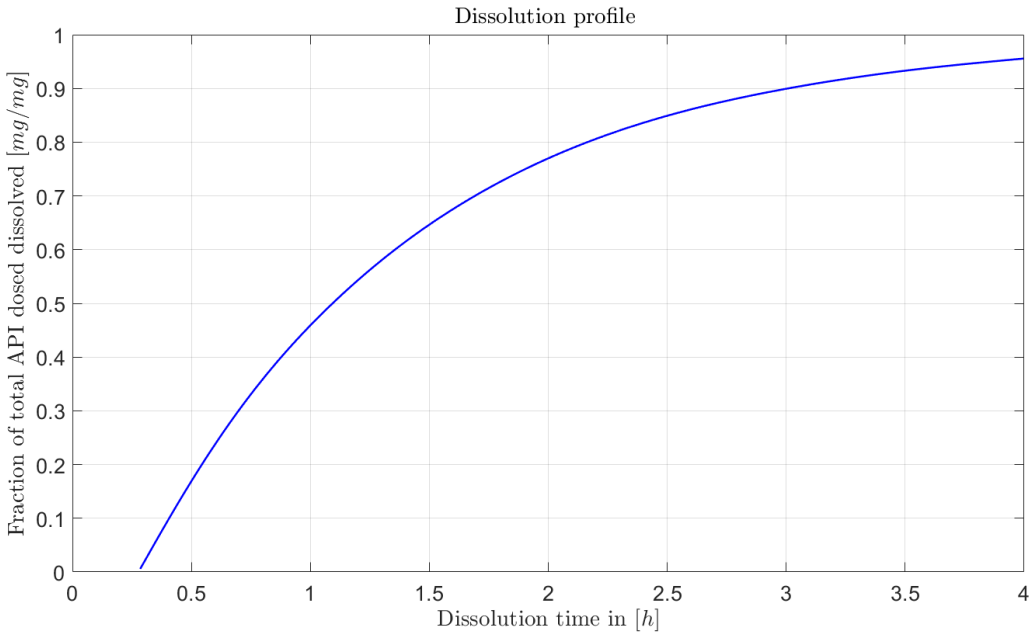

Figure 24: Dissolution profile showing the rate of release of a drug substance from the solid dosage form. Simulation with model input values set to their nominal value.

Figure 22 shows that the main effects are clearly the API mass flow rate ($\dot{m}_{API}$), as well as the compaction force F_{comp}. The high effect of $\dot{m}_{API}$ is explainable due to the fact that mass flow rate contributes to the API mass fraction of the final tablet. The composition of the final tablet is thereby affected and leads to a different dissolution kinetic. An API mass fraction of e.g. 20wt% is apparently leading to a different dissolution kinetic compared to a mass fraction of 5wt%. Even though the formulation is affected by different contributions of the mass flow rates, a percent wise normalization of the dissolution allows a comparability of the different simulation runs.

The first-order sensitivity indices are smaller than the total effects (Figure 23) for the physical output with a sum of 0.6 compared to the sum of the total-order indices of around 2. The effect on tablet disintegration is only recognizable after an extent of dissolution /dissolved API mass fraction of 50%, where it becomes obvious that the compaction force and the API mass flow rate are becoming mainly influential. This relates to the dissolution model where the first step towards solution is breaking down the tablet into smaller particles or granules, a process called disintegration.

By analyzing the total effect indices, very high sensitivity is detected for F_{comp}, μ_{API}, $\dot{m}_{API}$ and $\dot{m}_{Mannitol}$ implying that the t_{90} value is driven by an interaction between them. In terms of factor prioritization (FP) which is aiming at ranking the inputs in terms of their relative

contribution to output uncertainty, the best choice is to select F_{comp} followed by the API mass flow rate $\dot{m}_{API}$. Total-order sensitivity measures $S_{T_i} \geq S_i$ imply that there are higher-order interactions between input parameters that contribute to the output variability. The interaction between the parameters is depicted in Figure 25 by normalization of the total order index $S_{T,t_{90}}$ to 1.

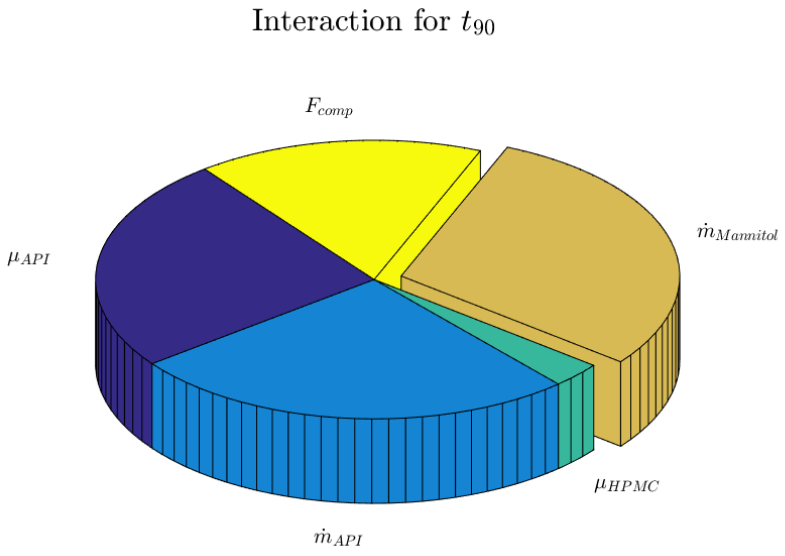

Figure 25: Pie chart of the interaction terms affecting the dissolution profile. $\boldsymbol{\omega_{Blender}}$ is neglected due to its minimal effect.

It is interesting that μ_{API} is not a main contributor to the dissolution, nevertheless it is considerably interacting with other inputs. The dissolution rate is affected by the particle size, since smaller particles yield higher reaction areas compared to the area of a larger particle, considering the same volume. This is important, because the diffusion kinetic of the active ingredient particle is related to its particle surface area (equation 42). Despite the fact that $\dot{m}_{Mannitol}$ is not a main contributor to the dissolution, its interaction with other model inputs is significant. This is related to its effect on the overall mass fraction of the tablet. Only higher-order indices would show the interaction among other parameters, nevertheless it is possible to account the effect of parameter interaction from model formulas.

To identify non-relevant input factors for the purpose of model reduction (often referred to as factor fixing FF) it is necessary to consider the total-order effects. This implies calculating total effect S_{T_i} sensitivity indices for individual input factors. Dealing with dynamic models it is necessary to calculate the indices time depending. If S_{T_i} is close to zero during the whole simulation, the input factor X_i does not influence the model output at any time. Therefore, the factor X_i can be fixed to any value within its range of variation, because it does not contribute to the output variance, neither singularly or in combination with other input factors. Taking this into account input factor $\omega_{Blender}$ can be set to any value within its defined distribution without affecting the dissolution kinetic.

3.3.1. Analysis of simulation convergence

Typically, the optimal number of samples at which the simulation produces accurate sensitivity measures is unknown. To set the optimal sample size is always case specific and depends on several attributes. The model itself is highly affecting the simulation outcome since non-linearity in the model equations as well as complexity of the model (i.e. recycles) attributes to the calculated indices. The convergence of Sobol indices is also affected by the chosen model outputs since their inner model calculation can be subject to non-linear behavior instead of linear relationships. Similarly, the number of input variables and their overall number are measures contributing to the convergence. Plotting key metrics of interest against the number of samples, allows to verify whether a sufficient sample size has been generated.

Based on the selection of 6 input factors and their distribution, a maximum sample size of 5200 was selected and generated using quasi-random numbers. To investigate the convergence additional simulation samples of 640, 1200, 1800, 2200, 3000 and 3840 were arbitrarily selected. Each of the sample sets containing the uncertain input parameters is processed for model output evaluation. The flowsheet simulated for a total of 28,800 seconds (corresponding to a dissolution kinetic of 8 hours) with data recorded at the simulation end and pre-determined time steps according to the dissolution profile. The model evaluation for 5200 samples took approximately 127h (using 6 cores) running on a 3.4 GHz Pentium 4 PC running Windows 7. Figure 26 to Figure 29 depict the first and total-order indices over an increasing sample size.

In Figure 26 it is shown, that the first-order indices converge till 2200 samples. At this sample size the first-order indices are no longer exceeding 1 which could occur by sampling errors when the Sobol method is approximating the sample variance. In case S_i is small and S_{T_i} is large, the variable X_i has important effect on the output but only through its interaction with other variables.

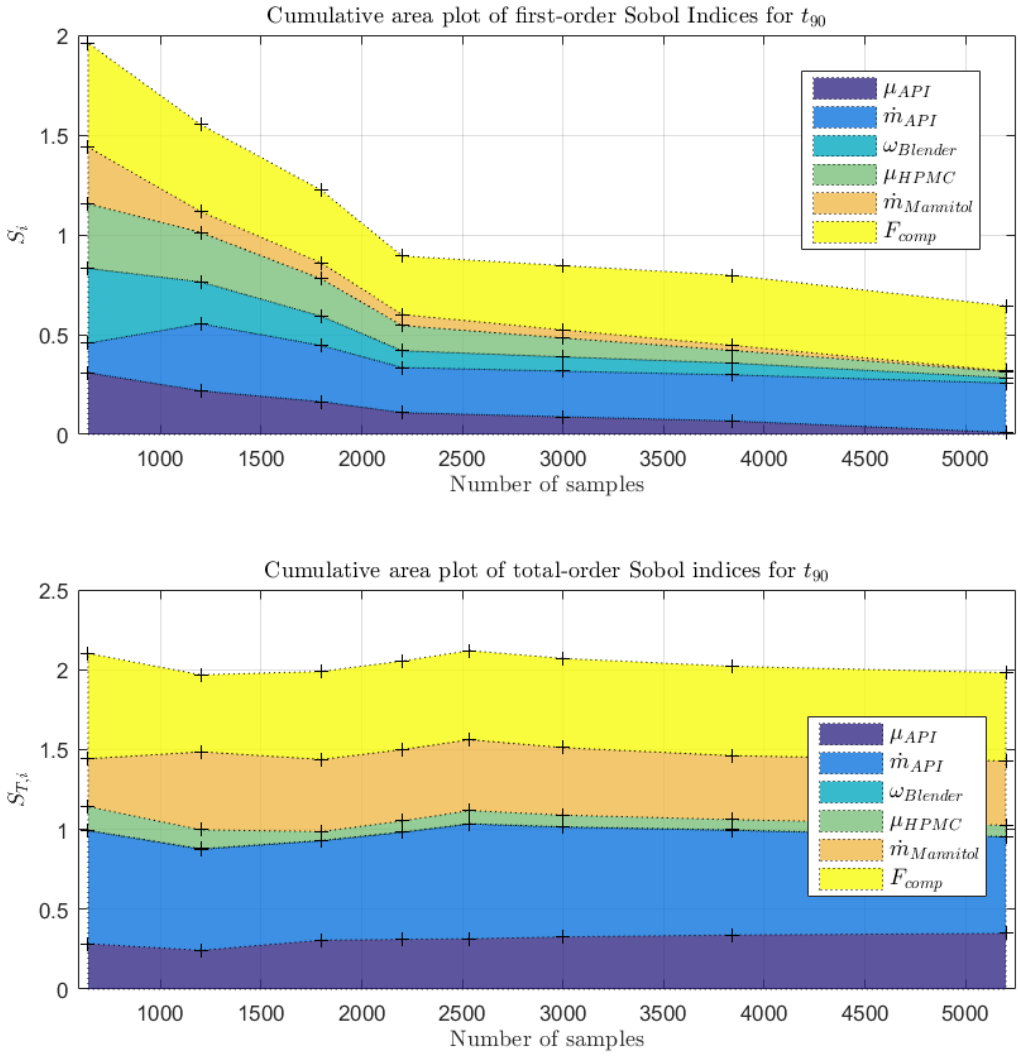

Figure 26: Variation of first and total order sensitivity indices along with increasing sample size. Evolution of the $\boldsymbol{t_{90}}$ over an increasing number of samples.

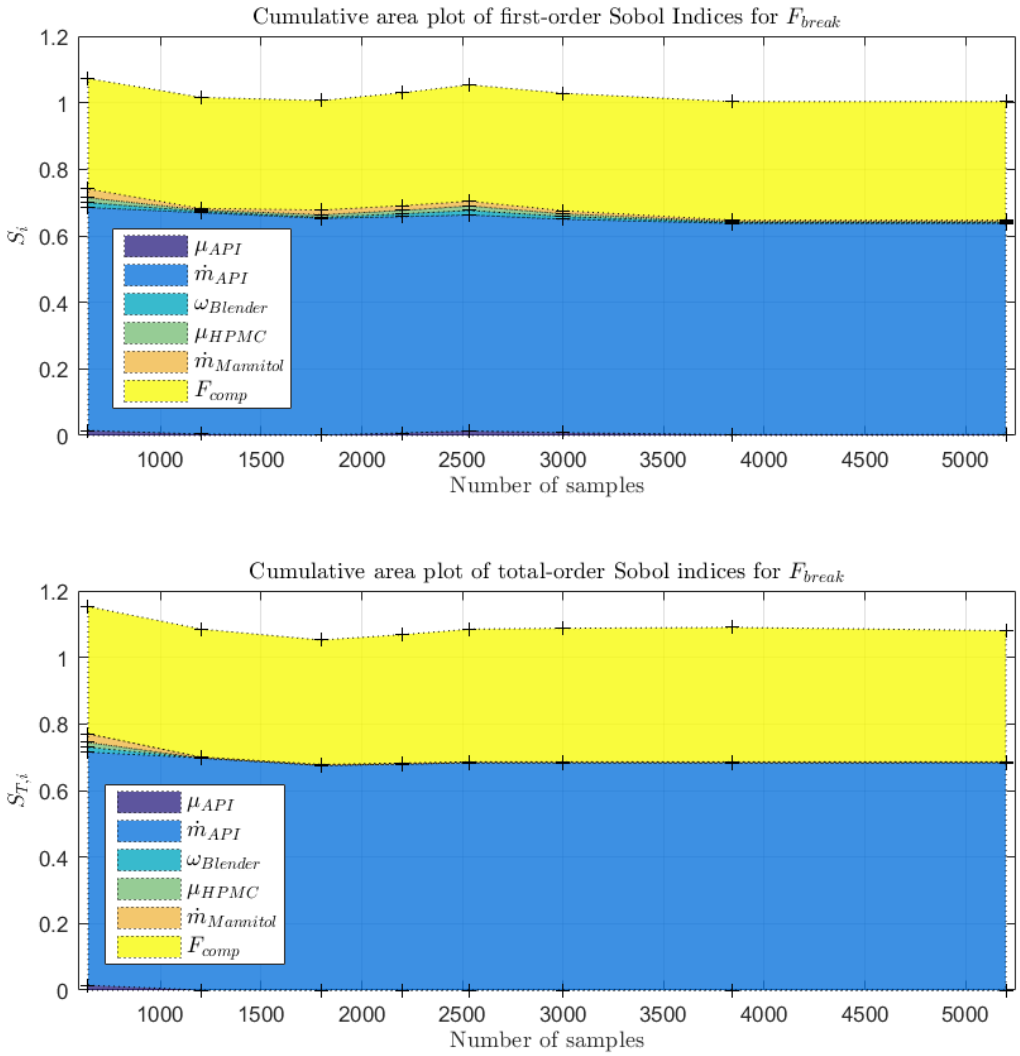

Figure 27: Variation of first and total order sensitivity indices along with increasing sample size. Evolution of the tablet hardness over an increasing number of samples.

Figure 26 to Figure 29 show that the sum of the first-order indices is exceeding a value of one for a lower number of samples. This is an indicator that the optimal number of samples is not yet reached. Starting at a sample size of 3600 the first-order indices start to converge starting to produce reliable results.

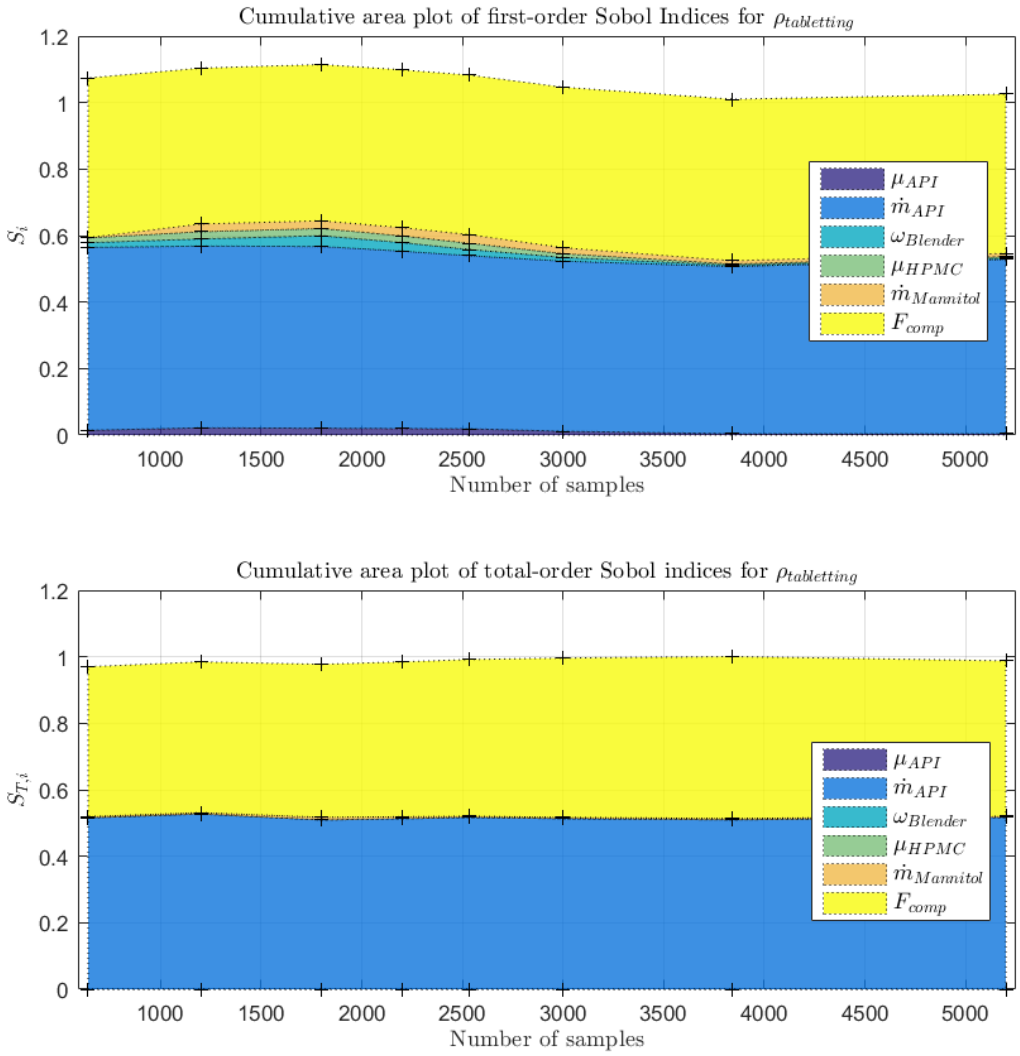

Figure 28: Evolution of the sum of the first and total order indices of the bulk density after tableting over an increasing sample size.

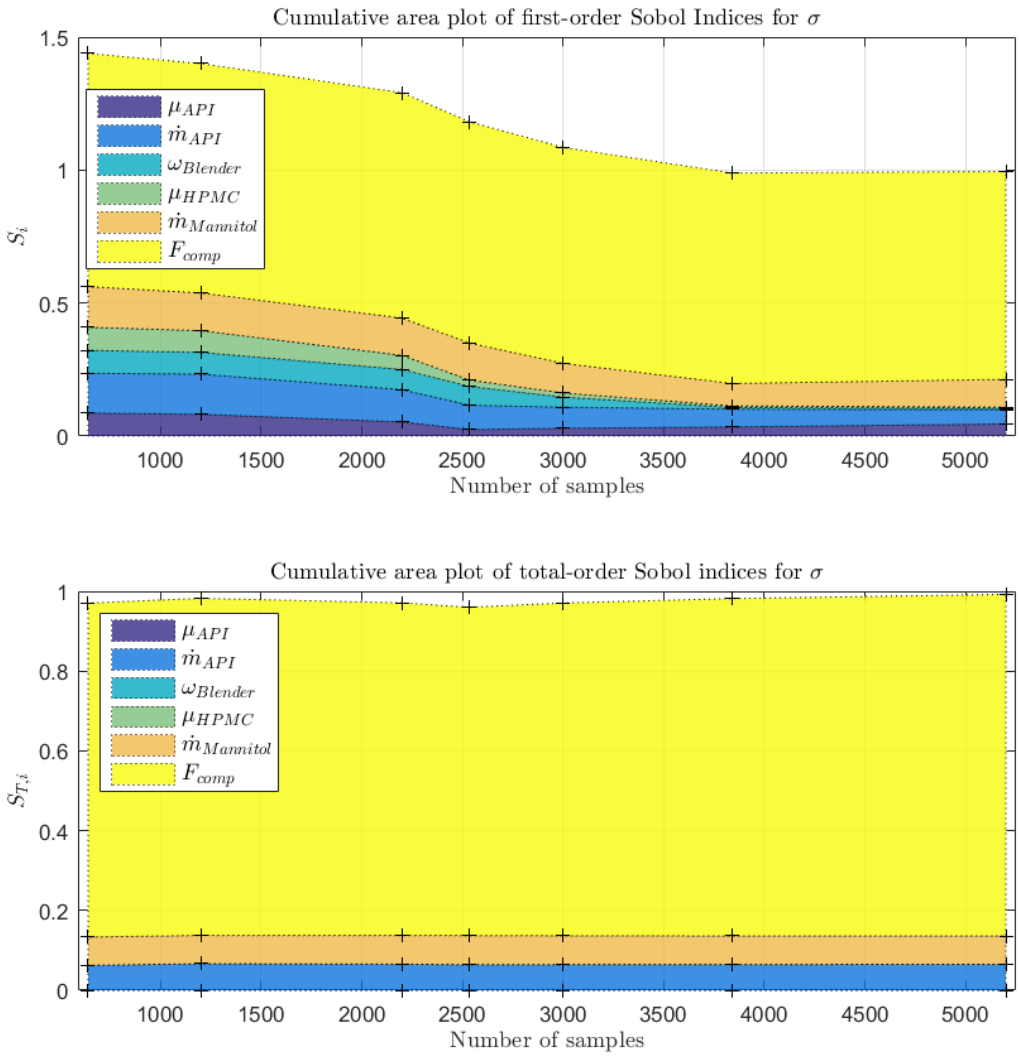

Figure 29: Evolution of the sum of the first order indices of the tablets tensile strength over an increasing sample size.

3.4.Morris method

As described in Chapter 1.3.2., there are two measures σ and μ^* describing the overall contribution to the output variance. The results are showing how the uncertainty in the output of the flowsheet model can be apportioned to different sources of uncertainty in its inputs. The subsequent paragraphs are discussing the effect of the model inputs for a total of 1600 simulation runs.

Hardness: As for the breaking force the subplot from Figure 30 indicated that F_{comp} and $\dot{m}_{API}$ have a larger μ^* than all the other parameters showing strong influence of these two parameters. A third influential parameter $\dot{m}_{Mannitol}$ shows a higher σ as well, indicating that it interacts with both other parameters but regarding the small values of σ in relation to μ^* the interaction is definitely low. The parameters found to be important on the breaking force are both of the mass flow rates contributing to the overall mass fraction and the compaction force. The mass flow rates are basically affecting the total composition of the tablet with regard to the mass fraction of each ingredient. Since each of the components has a different bulk density ρ_{bulk} which is contributing to the porosity, an affect onto the tablet hardness is observable. By utilizing the Morris screening method, the material properties of Mannitol and API were found to be insignificant to the breaking force, therefore their values could be fixed within their defined range.

Extent of lubrication: The extent of lubrication is basically only affected by the rotor speed of the blender showing high linear impact due the relatively small σ to μ^* ratio (Figure 30).

Tensile strength: Regarding the tensile strength, the main contributor is the compaction force followed by the mass flow rates. Due to the fact, that the breaking force is direct proportional to the tensile strength (equation 39 is only affected by the geometry of the tablet), it is not surprising that the μ^*-σ scatter plot looks similar since the tensile strength is calculated first.

The extent of lubrication which is directly affecting σ_{Lub} is basically only affected by the rotation rate of the blender. Although it looks like that both of the mass flow rates are influential as well, it should be noted that their effect is neglectable for the considered formulation. Without paying attention to the scaling of the axes (Figure 30), an impression of interaction among the mass flow rates is created.

Dissolution profile*:* Figure 31 indicated that $\dot{m}_{API}$ and $\dot{m}_{Mannitol}$ have a larger standard deviation σ than all the others, which concludes that a non-linear relationship between parameters and model outputs is more noticeable or that their interaction with other parameters is more evident. It is plausible to suspect that parameters with higher mean values μ^* have a higher possibility of presenting a larger standard deviation. These high ranking parameters with large standard deviation σ must be paid attention, since the high non-linearity of the model and/or the interaction with other parameters decreases the reliability of sensitivity classification (according to Figure 6 described by Loubière et al. [36]). An assessment only based on σ is a major disadvantage of the Morris method, since it prohibits the distinction of model non-linearity and interaction between parameters.

The impact on the dissolution profile is clearly affected by the uncertainty of the compaction force and the mass flow rates who are contributing highly to a different mass fraction of the tablet showing high interaction or non-linear behaviour. It is interesting to notice, that as dissolution progresses the effect of the particle size of the API is coming more and more into play the longer it takes to release the active ingredient. Nevertheless, the effect of μ_{API} is considered to be very small with almost no interaction among the other parameters. Regarding the dissolution profile, the originally 6 material and process parameters of the flowsheet model can be reduced to 4, reducing the computational effort by a third. That is one of the reasons for the broad application of the Morris screening method, as it could be used as a first step to lower computational demand.

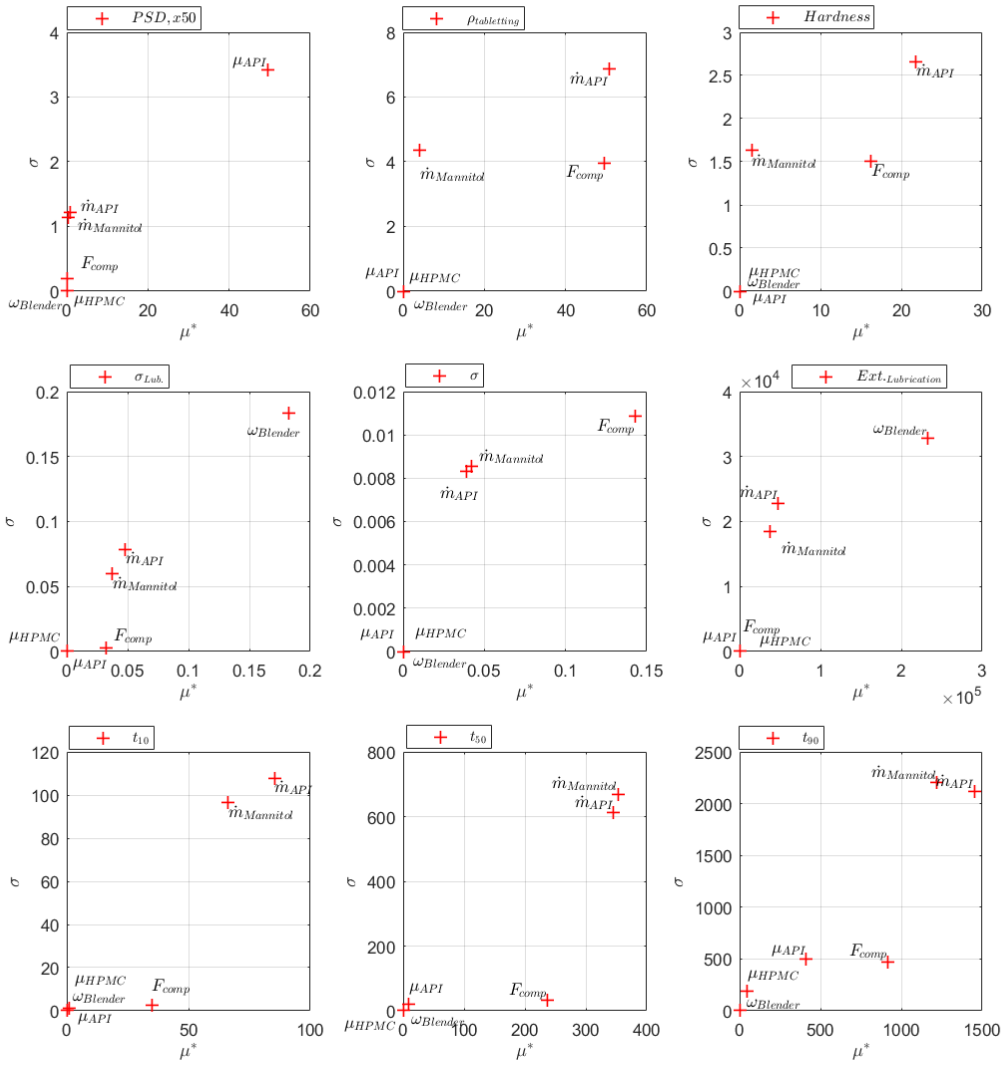

Figure 30: Scatter plots of the Morris screening results for $\boldsymbol{\mu^*}$-$\boldsymbol{\sigma}$ plane.

There is no contradiction that the values depicted in Figure 30 for σ are above the ones for μ^*. The mean is simply a measure of location, whereas the standard deviation is more generally a measure of spread. A smaller standard deviation indicates that more of the data is clustered about the mean, a larger one indicates the data are more spread out.

As seen from Figure 31, the results are containing negative elements, which can occur when the model is non-monotonic and calculated with equation 20. By computing μ_i, it can happen that some elementary effects may cancel each other out, which make the goal of ranking them in order of importance, difficult.

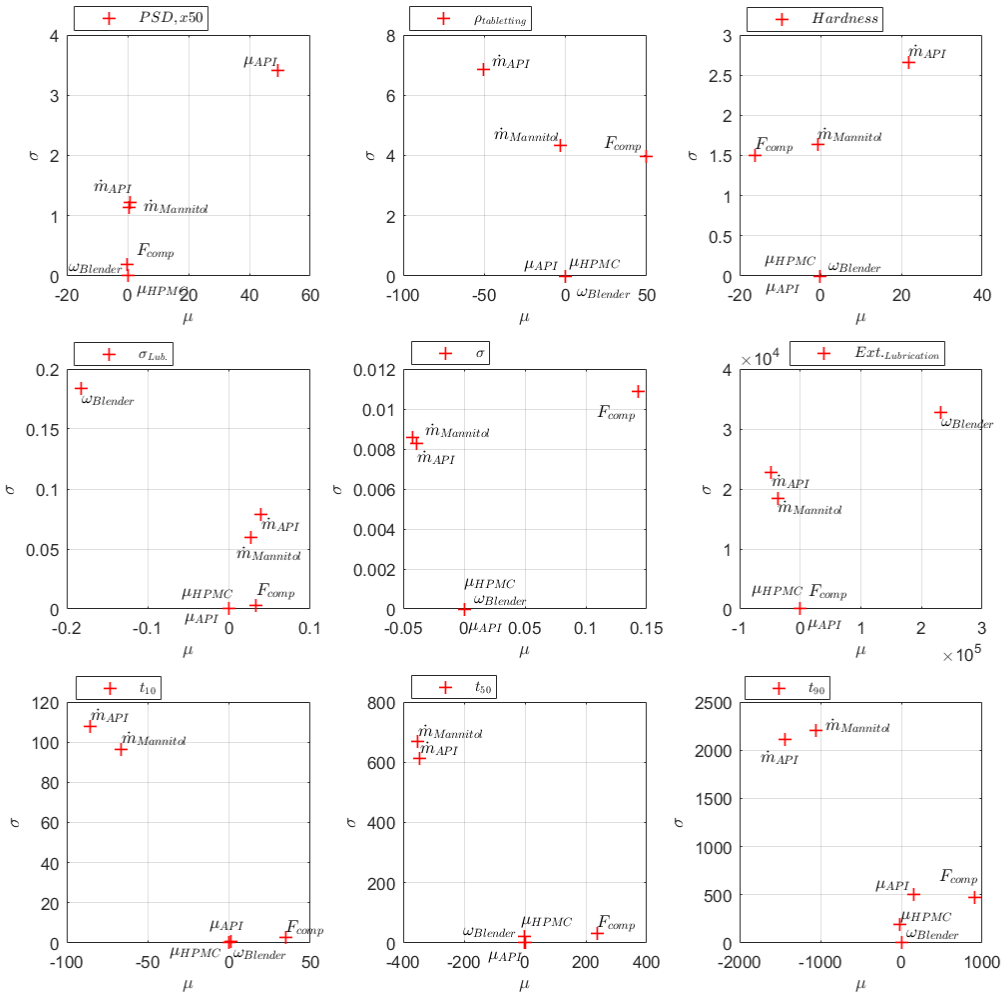

Figure 31: Scatter plots of the Morris screening results for $\boldsymbol{\mu}$-$\boldsymbol{\sigma}$ plane.

3.5. Impact of material and process parameters on product performance

With the statistical information provided by the GSA simulations (Table 5) it is possible to analyze the ranges of the dissolution profile. The dissolution behavior of the various direct compression formulations reveal considerable variations in its performance.

Table 5: Statistical output of the GSA simulation runs.

Parameter	Unit	Mean	Std. deviation	Minimum	Maximum	Median	$Q_{5\%}$	$Q_{95\%}$
ρ_{tablet}	kg/m^3	305.50	5.16	297.09	316.31	305.12	301.04	309.92
F_{break}	N	407.41	7.87	388.89	425.55	407.48	401.63	413.16
σ	MPa	1.84	0.05	1.79	2.13	1.82	1.81	1.84
σ_{Lub}	MPa	8.21	0.04	8.11	8.32	8.21	8.18	8.25
t_{10}	h	0.401	0.006	0.390	0.433	0.400	0.397	0.404
t_{20}	h	0.529	0.009	0.510	0.586	0.529	0.522	0.534
t_{30}	h	0.674	0.014	0.646	0.763	0.674	0.664	0.682
t_{40}	h	0.842	0.019	0.804	0.975	0.841	0.828	0.854
t_{50}	h	1.042	0.026	0.990	1.215	1.040	1.023	1.057
t_{60}	h	1.286	0.035	1.218	1.524	1.285	1.260	1.307
t_{70}	h	1.643	0.048	1.546	1.918	1.642	1.608	1.673
t_{80}	h	2.123	0.068	1.984	2.573	2.120	2.072	2.169
t_{90}	h	3.000	0.117	2.756	3.626	2.986	2.918	3.070

Based on the prior sensitivity analysis it is interesting to show how a change of the main influential process parameters is affecting the model output. Therefore, all the model inputs are set to their mean values except for the considered main effects. Figure 32 shows two of the model output ensembles with the effect of F_{comp} and $\dot{m}_{API}$, - basically describing a local sensitivity analysis. Table 6 depicts the simulation configuration of the two CPPs which are mainly influential to the dissolution kinetic. The mean relates to the standard values, with the extremes represented by their minimum and maximum values (comparable to the GSA inputs in Table 1).

Table 6: Input configuration for the dissolution curves.

Parameter	Unit	Mean	Minimum	Maximum
$\dot{m}_{API}$	kg/h	0.42	0.007	0.77
F_{comp}	kN	7	6	8

For the graphs in Figure 32 combinations of the API mass flow rate and the compaction force were selected to show how the different values affect the deviation of the dissolution kinetic. To observe the interaction among the two variables and not their quantitative attribution to the dissolution (provided by GSA), simulations have been run with extreme values specified in Table 6.

Higher compression forces during tableting result in longer dissolution time, whereas a higher API mass fraction leads to a decrease. A higher compaction of the tablet results in an extended release of the active pharmaceutical ingredient. The effect of the API mass flow rate can be explained similarly by a contribution to the overall API mass fraction to the tablets porosity.

The small but still significant effect (shown by GSA) of the particle size distribution of the API (μ_{API}) on the dissolution kinetic is caused by the fact that smaller particles and therefore their area is relatively increasing, leading to higher surface area for diffusion.

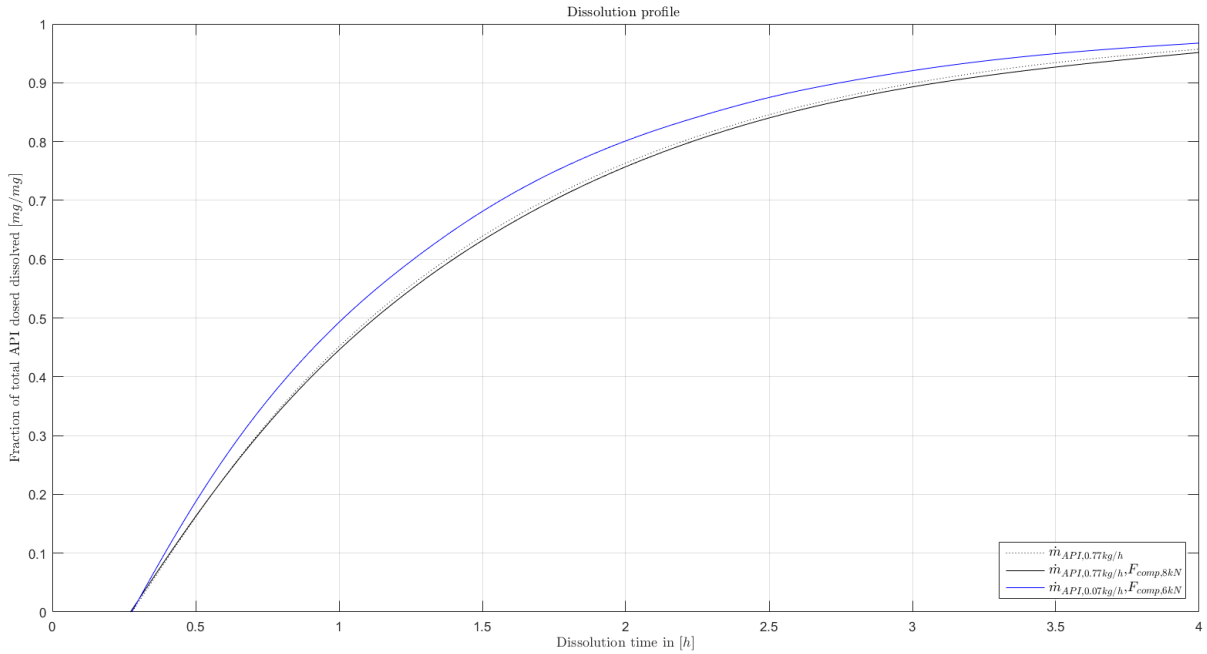

Figure 32: Dissolution profiles of the drug for various direct compression formulations.

4. Conclusion

In this work a FIFO based hopper model with variable dead-time delay was developed. The model allowed studying the delayed discharge of mass fraction depending on the inlet trajectories. The factors investigated are the mass fraction of solid material in the hopper feed. The effect of time delay is mainly affected by the mass holdup within the hopper. Despite the fact that gProms is not established to use it for time discrete models, an implementation approach fitting our needs has been implemented. The hopper model was part of the established direct compaction flowsheet model and proved to be feasible for the process simulation.

Furthermore, this study evaluated a global sensitivity analysis for a direct compaction flowsheet model. This work demonstrates the benefit of using model-based approaches for determining the influence of material, formulation and process parameters on critical quality attributes, such as dissolution profile, tensile strength and breaking force. The list of potential influential factors can be reduced by using GSA. Using the introduced approaches allows to detect critical material (CMA) and critical process parameters (CPP) which are influential to the performance of a drug product. The work provides a practical guideline in assisting users to perform GSA on a gProms direct compaction manufacturing flowsheet. Knowledge of the critical process parameter is an important concern, regardless of physical design of experiments or model-based approaches. Proper knowledge of the influence of process and model parameters is allowing useful information regarding which of these parameters should be considered important. Since all model inputs are subject to sources of uncertainty including errors of measurement or conceptual uncertainty, there is a clear benefit in determining the critical quality attributes based on numerical flowsheet simulation. These uncertainties in the model assumptions and specifications impose limits on the confidence in the model output and pave the way for this still relatively new approach to the pharmaceutical industry.

In terms of quantifying interactions among the input parameters the results of the Morris method and an ANOVA based Sobol method are examined. The interaction of the Sobol method for each input parameter was estimated by the difference between its first-order and total-order sensitivity index. Based on the Sobol's first-order sensitivity index S_i, the compaction force, mass flow rates and API particle size could be found to be the primary contributors to the variance of the tensile strength, breaking force and dissolution profile. The Sobol's variance decomposition approach also captures the influence of the interaction among parameters on a

model output. It could be obtained, that particle size distribution of HPMC (μ_{HPMC}) is a parameter that has a neglectable impact on all of the investigated model outcomes.
The GSA reveals that the composition of the various formulations is considerable affecting the dissolution behavior. Despite an expected relation of the lubrication on the dissolution characteristics the model is not yet capable to map these to real world dynamics.

By comparing the two methods, it is observable that the Morris method worked well as an interaction measure, which is consistent with the Sobol method at greatly reduced computational costs. The computational costs of pharmaceutical process models may be the most important obstacle that impedes the application of the variance-based GSA methods. Considering the computational costs, the 1600 runs needed for the Morris method are preferable to the 5200 runs needed for the same data with Sobol's method. Therefore, the Morris method provides a more practical approach for the analysis of models including large numbers of parameters or computational time demanding models. Nevertheless, convergence examination shows, that there is little benefit in running the Sobol method for sample sizes greater than 2500, since the correlation remains similar for higher sample sizes. In cases where assessing the relative reduction in output variance is required, variance based approaches such as the Sobol method must be used. Both methods can be used together, potentially reducing the computational costs by first performing parameter screening using the Morris method. Non-influential parameters can be filtered out reducing the dimension of the parameter space, allowing further analysis with reduced computational costs.

Other processes such as granulation, which are including hundreds of variables have an even more complex behavior which cannot be predicted or solved analytically [53]. Numerical GSA simulation offers a solution that can help to gain knowledge of certain process steps via mechanistic models. Model-based simulations could provide a cost-effective alternative to the early phase validation and/or sophisticated process investigation.

Furthermore, the calculation of global sensitivity could offer several opportunities for advanced control applications [7]. The derived results from both approaches for identifying influential variables could be promising for further model validation and control strategies. With a knowledge of the involved process parameters and their interaction, a plant control could be established since MIMO systems are highly challenging for a control engineer to meet specific quality criteria. But most important such a sensitivity analysis of a flowsheet model provides

further insight to the dynamic model behavior. These models can be used as soft-sensors for the prediction of process variables which are not directly measurable but required for the end-product. The flowsheet models may not be capable to match all the predictions with real world results. Since most of the models imply simplifications and idealizations, they are useful to map reality by some extent.

Nomenclature

Acronyms

ANOVA	Analysis of variance
API	Active pharmaceutical ingredient
BF	Breaking force
CMA	Critical material attribute
CPP	Critical process parameter
CQA	Critical quality attribute
DEM	Discrete element method
DoE	Design of experiments
FAST	Fourier amplitude sensitivity test
FDA	Food and Drug Administration
FIFO	First in first out
GSA	Global sensitivity analysis
GUI	Graphical user interface
HU	Hold-up
ICH	International Council for Harmonisation of Technical Requirements for Pharmaceuticals for Human Use
LHC	Latin hyper cube
LOD	Loss on drying
MPC	Model predictive control
OFAT	One-factor-at-a-time
ODE	Ordinary differential equation
OOS	Out of specification
PDF	Probability density function
PSD	Particle size distribution
PP	Process parameter
QbD	Quality by design
QTPP	Quality target product profile

Greek symbols and math

μ_{API}	Particle size distribution API
μ_{HPMC}	Particle size distribution HPMC
	mean of the distribution of the absolute values
$\rho_{tablett}$	Relative density of the tablet after compaction
σ	Tensile strength (without lubrication)
$\sigma_{Lubr.}$	Tensile strength (including lubrication)
$\omega_{Blender}$	Rotation rate of the blender
F_{break}	Tablet breaking force/tablet hardness
$F_{comp.}$	Compaction pressure
$\dot{m}_{API}$	Mass flow rate API
$\dot{m}_{Mannitol}$	Mass flow rate Mannitol
M	Size of the hopper model ring buffer
S	First-order sensitivity index
S_T	Total-order sensitivity index
t_{10}	Dissolution time till 10wt% of solid drug in dissolution
t_d	Delay time regarding the hopper model
$x50$	50% quantile of the particle size distribution

List of Figures

List of Tables

References

[1] T. Ervasti, S.P. Simonaho, J. Ketolainen, P. Forsberg, M. Fransson, H. Wikström, et al., Continuous manufacturing of extended release tablets via powder mixing and direct compression, Int. J. Pharm. 495 (2015) 290–301.

[2] M.C. Martinetz, J. Rehrl, I. Aigner, S. Sacher, J. Khinast, A Continuous Operation Concept for a Rotary Tablet Press Using Mass Flow Operating Points, Chemie-Ingenieur-Technik. 89 (2017) 1006–1016.

[3] S. Moghtadernejad, M.S. Escotet-Espinoza, S. Oka, R. Singh, Z. Liu, A.D. Román-Ospino, et al., A Training on: Continuous Manufacturing (Direct Compaction) of Solid Dose Pharmaceutical Products, J. Pharm. Innov. (2018) 1–33.

[4] Ich, Q8(R2) Pharmaceutical Development, Food Drug Adm. 8 (2009) 1–29.

[5] F. Boukouvala, V. Niotis, R. Ramachandran, F.J. Muzzio, M.G. Ierapetritou, An integrated approach for dynamic flowsheet modeling and sensitivity analysis of a continuous tablet manufacturing process, Comput. Chem. Eng. 42 (2012) 30–47.

[6] J. Rehrl, A. Gruber, J.G. Khinast, M. Horn, Sensitivity analysis of a pharmaceutical tablet production process from the control engineering perspective, Int. J. Pharm. 517 (2017) 373–382.

[7] I.M. Cotabarren, D.E. Bertín, V. Bucalá, J. Piña, Feedback control strategies for a continuous industrial fluidized-bed granulation process, Powder Technol. 283 (2015) 415–432.

[8] T. Glaser, C.F.W. Sanders, F.Y. Wang, I.T. Cameron, J.D. Litster, J.M.-H. Poon, et al., Model predictive control of continuous drum granulation, J. Process Control. 19 (2009) 615–622.

[9] A. Bück, S. Palis, E. Tsotsas, Model-based control of particle properties in fluidised bed spray granulation, Powder Technol. 270 (2015) 575–583.

[10] S. Chatterjee, FDA Perspective on Continuous Manufacturing, IFPAC Annu. Meet. (2012) 21.

[11] US Food and Drug Administration, https://www.accessdata.fda.gov/scripts/cdrh/cfdocs/cfcfr/CFRSearch.cfm?fr=210.3, (2017).

[12] J. Kruisz, J. Rehrl, S. Sacher, I. Aigner, M. Horn, J.G. Khinast, RTD modeling of a continuous dry granulation process for process control and materials diversion, Int. J. Pharm. 528 (2017) 334–344.

[13] X. Zhang, M.N. Trame, L.J. Lesko, S. Schmidt, Sobol Sensitivity Analysis : A Tool to Guide the Development and Evaluation of Systems Pharmacology Models, CPT Pharmacometrics Syst. Pharmacol. 4 (2015) 1–4.

[14] R. Martin, I. Lazakis, S. Barbouchi, L. Johanning, Sensitivity analysis of offshore wind farm operation and maintenance cost and availability, Renew. Energy. 85 (2016) 1226–1236.

[15] Y. Tang, P. Reed, K. Van Werkhoven, T. Wagener, Advancing the identification and evaluation of distributed rainfall-runoff models using global sensitivity analysis, Water Resour. Res. 43 (2007) 1–14.

[16] C. Zhang, J. Chu, G. Fu, Sobol's sensitivity analysis for a distributed hydrological model of Yichun River Basin, China, J. Hydrol. 480 (2013) 58–68.

[17] J. Nossent, P. Elsen, W. Bauwens, Sobol sensitivity analysis of a complex environmental model, Environ. Model. Softw. 26 (2011) 1515–1525.

[18] I.M. Sobol, Global sensitivity indices for nonlinear mathematical models and their Monte Carlo estimates, Math. Comput. Simul. 55 (2001) 271–280.

[19] A. Saltelli, S. Tarantola, F. Campolongo, M. Ratto, Sensitivity Analysis in Practice: A Guide to Assessing Scientific Models, Wiley, 2004.

[20] N. a S. Hamm, J.W. Hall, M.G. Anderson, Variance-based sensitivity analysis of the probability of hydrologically induced slope instability, Comput. Geosci. 32 (2006) 803–817.

[21] T. Homma, A. Saltelli, Importance measures in global sensitivity analysis of nonlinear models, Reliab. Eng. Syst. Saf. 52 (1996) 1–17.

[22] A. Saltelli, P. Annoni, How to avoid a perfunctory sensitivity analysis, Environ. Model. Softw. 25 (2010) 1508–1517.

[23] L.U. July, Simlab Manual v2, Simlab. (2008).

[24] J. Norton, An introduction to sensitivity assessment of simulation models, Environ. Model. Softw. 69 (2015) 166–174.

[25] A. Saltelli, P. Annoni, I. Azzini, F. Campolongo, M. Ratto, S. Tarantola, Variance based sensitivity analysis of model output. Design and estimator for the total sensitivity index, Comput. Phys. Commun. 181 (2010) 259–270.

[26] R. Broed, P.-A. Ekström, Sensitivity Analysis Methods and a Biosphere Test Case Implemented in EIKOS, Posiva Work. Rep. 31 (2006) 84.

[27] a Saltelli, Making best use of model valuations to compute sensitivity indices, Comput. Phys. Commun. 145 (2002) 280–297.

[28] F. Sarrazin, F. Pianosi, T. Wagener, Global Sensitivity Analysis of environmental models: Convergence and validation, Environ. Model. Softw. 79 (2016) 135–152.

[29] K. Chan, A. Saltelli, S. Tarantola, Sensitivity Analysis of Model Output: Variance-based Methods Make the Difference, (1997) 261–268.

[30] A.-T. Nguyen, S. Reiter, A performance comparison of sensitivity analysis methods for building energy models, Build. Simul. 8 (2015) 651–664.

[31] F. Qin, Y. Zhao, X. Shi, S. Xu, D. Yu, Sensitivity and uncertainty analysis for the DeNitrification-DeComposition model, a case study of modeling soil organic carbon dynamics at a long-term observation site with a rice-bean rotation, Comput. Electron. Agric. 124 (2016) 263–272.

[32] F. Campolongo, J. Cariboni, Sensitivity analysis: how to detect important factors in large models, Eur. Comm. Jt. Res. Centre, Ispra (VA), Italy. (2007).

[33] F. Campolongo, A. Saltelli, J. Cariboni, From screening to quantitative sensitivity analysis. A unified approach, Comput. Phys. Commun. 182 (2011) 978–988.

[34] M.D. Morris, Factorial plans for preliminary computational experiments, Technometrics. 33 (1991) 161–174.

[35] F. Campolongo, J. Cariboni, A. Saltelli, An effective screening design for sensitivity analysis of large models, Environ. Model. Softw. 22 (2007) 1509–1518.

[36] P. Loubière, A. Jourdan, P. Siarry, R. Chelouah, A sensitivity analysis method for driving the Artificial Bee Colony algorithm's search process, Appl. Soft Comput. J. 41

(2016) 515–531.

[37] S. Lakio, P. Tajarobi, H. Wikström, M. Fransson, J. Arnehed, T. Ervasti, et al., Achieving a robust drug release from extended release tablets using an integrated continuous mixing and direct compression line, Int. J. Pharm. 511 (2016) 659–668.

[38] R. Gul, S. Bernhard, Parametric uncertainty and global sensitivity analysis in a model of the carotid bifurcation: Identification and ranking of most sensitive model parameters, Math. Biosci. 269 (2015) 104–116.

[39] V. Niotis, Application of dynamich Global Sensitivity Analysis in Complex Systems, University of Medicine and Dentistry of New Jersey, 2012.

[40] H. Monod, C. Naud, D. Makowski, Uncertainty and sensitivity analysis for crop models, Work. with Dyn. Crop Model. (2006) 55–100.

[41] C. Haan, D. Storm, T. Al-Issa, Effect of parameter distributions on uncertainty analysis of hydrologic models, Trans. …. 41 (1998) 65–70.

[42] J. C Helton, Uncertainty and Sensitivity Analysis Techniques for Use in Performance Assessment for Radioactive Waste Disposal, Reliab. Eng. Syst. Saf. 42 (1993) 327–367.

[43] M.D. McKay, R.J. Beckman, W.J. Conover, Comparison of Three Methods for Selecting Values of Input Variables in the Analysis of Output from a Computer Code, Technometrics. 21 (1979) 239–245.

[44] W.R. Ketterhagen, B.C. Hancock, Optimizing the design of eccentric feed hoppers for tablet presses using DEM, Comput. Chem. Eng. 34 (2010) 1072–1081.

[45] W.R. Ketterhagen, J.S. Curtis, C.R. Wassgren, B.C. Hancock, Predicting the flow mode from hoppers using the discrete element method, Powder Technol. 195 (2009) 1–10.

[46] P. Toson, J.G. Khinast, Impulse-based dynamics for studying quasi-static granular flows: Application to hopper emptying of non-spherical particles, Powder Technol. 313 (2017) 353–360.

[47] S. Albaraki, S.J. Antony, How does internal angle of hoppers affect granular flow? Experimental studies using digital particle image velocimetry, Powder Technol. 268 (2014) 253–260.

[48] Process Systems Enterprise Limited, Vertical Blender Documentation, 2017.

[49] P. Enterprise, Tablet dissolver, gSOLIDS Model Doc. (2014) 1–8.

[50] Process Systems Enterprise Limited, In-vitro Model Documentation, 2017.

[51] P.S. Enterprise, gSOLIDS Model Documentation Hopper, (2013) 1–15.

[52] F. Pianosi, F. Sarrazin, T. Wagener, A Matlab toolbox for Global Sensitivity Analysis, Environ. Model. Softw. 70 (2015) 80–85.

[53] M. Dosta, S. Heinrich, J. Werther, Fluidized bed spray granulation: Analysis of the system behaviour by means of dynamic flowsheet simulation, Powder Technol. 204 (2010) 71–82.

Appendix